

# HABITATS IN THE PRE-TAGHANIC (GIVETIAN, MIDDLE DEVONIAN) MUDDY CARBONATE RAMP AT MIŁOSZÓW (HOLY CROSS MOUNTAINS, POLAND): GEOCHEMICAL AND MICROFACIES EVIDENCE

Agnieszka PISARZOWSKA\* , Grzegorz RACKI & Michał RAKOCIŃSKI

*Institute of Earth Sciences, Faculty of Natural Sciences, University of Silesia in Katowice,  
Będzińska 60, 41-200 Sosnowiec, Poland;*

*e-mails: [agnieszka.pisarzowska@us.edu.pl](mailto:agnieszka.pisarzowska@us.edu.pl), [grzegorz.racki@us.edu.pl](mailto:grzegorz.racki@us.edu.pl), [michal.rakocinski@us.edu.pl](mailto:michal.rakocinski@us.edu.pl)*

*\* Corresponding author*

Pisarzowska, A., Racki, G. & Rakociński, M., 2022. Habitats in the Pre-Taghanic (Givetian, Middle Devonian) muddy carbonate ramp at Miłoszów (Holy Cross Mountains, Poland): geochemical and microfacies evidence. *Annales Societatis Geologorum Poloniae*, 92: 381–409.



**Abstract:** The well-known fossiliferous and lithologically variable Middle Devonian Shaly-Calcareous Skąły Formation in the Łysogóry Region (northern part of the Holy Cross Mountains, central Poland) was studied for the first time in terms of elemental geochemistry, carbon isotope stratigraphy and limestone microfacies. Three Lower to Middle Givetian marly-limestone successions, exposed at Miłoszów, represent middle to outer facies belts of the vast carbonate ramp, characterized by very rich epifaunal and infaunal benthic life in muddy, oxic, eutrophic, and photic zone habitats. Brachiopods and occasionally corals (in mesophotic association), erect branching bryozoans, and tiny crinoids played a leading role among flourishing sessile suspension-feeders. High-energy storm events, possibly even a tsunami, during the brief Early Givetian time strengthened a prolific carbonate ooze delivery system from shallow ramp areas, including restricted back-ramp lagoons and a variety of organic build-ups, populated by corals and stromatoporoids. The ecologically mixed skeletal grain association is characterized by the rich occurrence of a typical lagoonal biota, calcispheres and amphiporoids. The effective carbonate factory declined stepwise regionally during the Middle Givetian because of an intermittent progradation of the deltaic system of the Świętomarz Beds, linked with climate cooling and the activation of block movements. The regional carbonate crisis resulted in the demise of diverse benthic life, including the prolific calcified microbiota. The higher Skąły Formation succession, deposited between the important Kačák and Taghanic bioevents, is noticeable for a background carbon-isotope pattern in carbonate and organic matter signatures, with the baseline  $\delta^{13}\text{C}_{\text{carb}}$  values between 1‰ and 2‰. The microfacies and chemostratigraphic data confirm that at least the lower *pumilio* bioevent was not recorded in the Łysogóry Region.

**Key words:** Carbon isotope chemostratigraphy, elemental geochemistry, limestone microfacies, carbonate ramp, Skąły Formation, Middle Devonian, Łysogóry Region, Holy Cross Mountains.

*Manuscript received, 8 August 2022, accepted 12 November 2022*

## INTRODUCTION

The Middle Devonian was an epoch of significant changes in atmospheric  $\text{pCO}_2$ , temperature (Simon *et al.*, 2007; Joachimski *et al.*, 2009), and sea-level (Becker *et al.*, 2016, 2020; Brett *et al.*, 2020). For example, mid-Devonian changes in  $\text{pCO}_2$ , brief warming and marine transgression were linked to the metamorphic  $\text{CO}_2$  degassing during the Acadian Orogeny (Acadian decarbonation; Stewart and Ague, 2018). On the basis of the magnitude and duration of major taxa extinctions, Devonian bioevents were classified from 1st- to 4th-order (Becker *et al.*, 2016). The Givetian stage includes four various orders of bioevents and the same

number of 3rd-order sea-level oscillations (Brett *et al.*, 2020).

The Taghanic crisis, at the end of the Middle Givetian to the beginning of the Upper Givetian (for the definitions of sub-stages see Becker *et al.*, 2020), is an example of a second-order event, connected with abrupt sedimentary changes, faunal overturns, and at least two transgressive pulses (House, 2002; Baird and Brett, 2008; Aboussalam and Becker, 2011; Zambito *et al.*, 2012; McGhee *et al.*, 2013). Prior to the Taghanic event, two dark, organic-rich levels with mass occurrences of minute brachiopods

“*Terebratula*” *pumilio* were documented in several successions in Germany and Morocco. The prolific brachiopods in fact represent, after Struve (1992), two genera *Ense* (2 species) and *Yekerpene* (see also García-Alcalde, 2010). These Middle Givetian coquinoid horizons have been named the lower and upper *pumilio* events (Lottmann, 1990a). The lower event falls in the higher part of the *varcus-rhenanus* conodont Zone, the upper at the base of the *ansatus* Zone (= Middle *varcus* Zone). The *pumilio* events reflect short-term transgressions and eutrophication and periods of faunal blooms (House 2002; Aboussalam and Becker 2011; Becker *et al.*, 2012). The presence of event-specific conodont genera (*Ancyrolepis*, *Latericriodus*) indicates the breaking of palaeobiogeographic barriers between eastern North America and western Gondwana/Europe (Aboussalam and Becker, 2011).

The Taghanic and *pumilio* events also were associated with a perturbation in the carbon cycle (Buggisch and Joachimski, 2006; Yans *et al.*, 2007). The record of these worldwide ecosystem changes, as well as the times preceding them, is still poorly understood in comparison to the Late Devonian events (see Becker *et al.*, 2020).

In this context, the fossiliferous and lithologically variable Middle Devonian Shaly-Calcareous Skały Formation (for definition see Racki *et al.*, 2022a) in the Łysogóry Region (northern part of the Holy Cross Mountains, central Poland) was investigated for the first time in terms of geochemistry (both elemental and stable isotopes) and limestone microfacies. Here, the authors present a multi-disciplinary study of the Lower–Middle Givetian marls and limestones, belonging to the upper part of the Skały Fm in Miłoszów sites, together with the basal marly shales of the

Świętomarz Beds (Fig. 1A, B; Halamski *et al.*, 2022). Only two somewhat enigmatic, *pumilio* bioevents are known in the Lower–Middle Givetian timespan (Becker *et al.*, 2020). The present authors reconstruct the changing environmental conditions in the Łysogóry carbonate ramp during the pre-Taghanic crisis period, and address the issue of its decline and whether the *pumilio* events were recorded in the studied sections.

## GEOLOGICAL SETTING

All samples were collected from outcrops, situated in the Miłoszów Forest between the Nieczulice, Cząstków, and Pokrzywianka Dolna villages, near Nowa Słupia in the Bodzentyn Syncline (Halamski, 2022, fig. 1B). This area, situated ca. 2.5 km west from well-known exposures in the Grzegorzowice-Skały section (Pajchłowa, 1957; Malec and Turnau, 1997; Halamski, 2022, fig. 1C), is characterized by intense fault tectonics, associated with the nearby major transverse Łysogóry Fault (Fig. 1B). Its detailed geological description, as well as that of the sections exposed mainly because of excavations in 2017–2019, are described in Halamski *et al.* (2022).

Limestones, marly limestones, and marly shales (claystones) of the Skały Fm, sporadically rich in diverse skeletal material (e.g., brachiopods, corals, crinoids), occur in the Miłoszów 0 (M0), Miłoszów 1 (M1), and Miłoszów 2 (M2) sections. Of these, only M0 is still available as an outcrop in the forest road escarpment (Fig. 1C). The Skały Fm in the M1 section was divided into two lithostratigraphic units (Fig. 2), a limestone unit (M1-Ia, Ib) and an overlying marly shale unit (M1-IIa, IIb). The Świętomarz Beds overlie

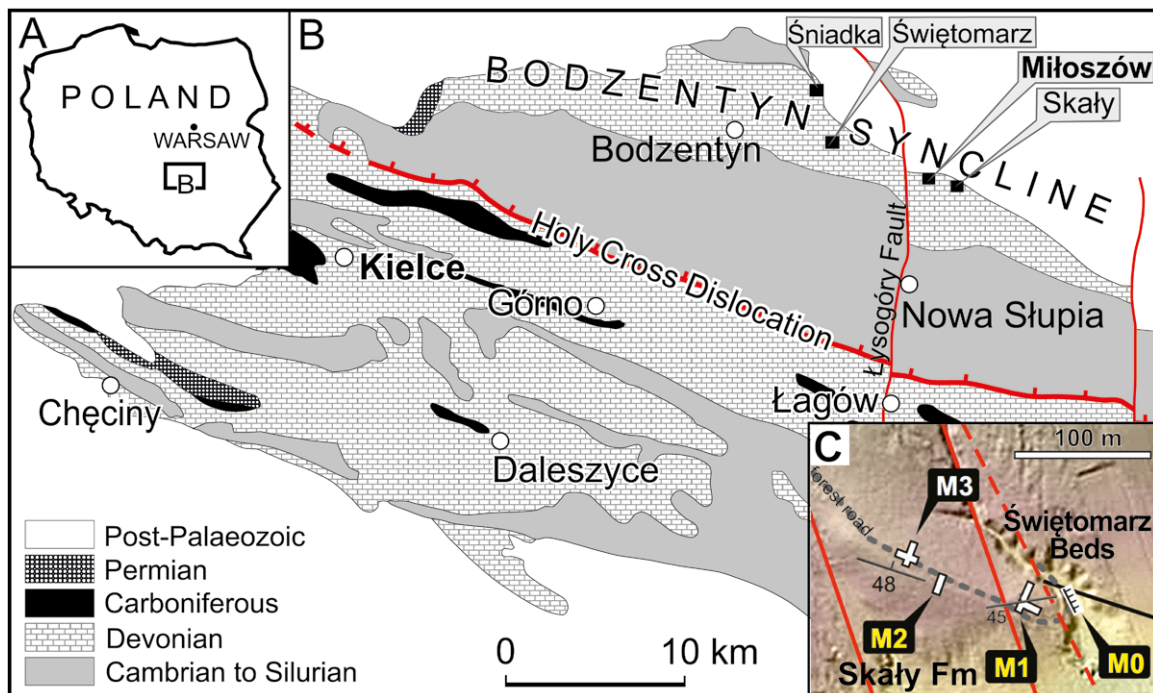


**Fig. 1.** Geological context of the study. **A, B.** Location of the Holy Cross Mountains in Poland (**A**) and the Skały Formation successions in the northeastern Holy Cross Mountains (**B**). **C.** Lidar image of the Miłoszów Forest with marked outcrops M0, M1, and M2, sampled for geochemical studies (yellow), and M3 (unstudied, white), and tectonic structures (based on figs 1B and 3A from Halamski *et al.*, 2022); red line – faults, dashed line – forest road.

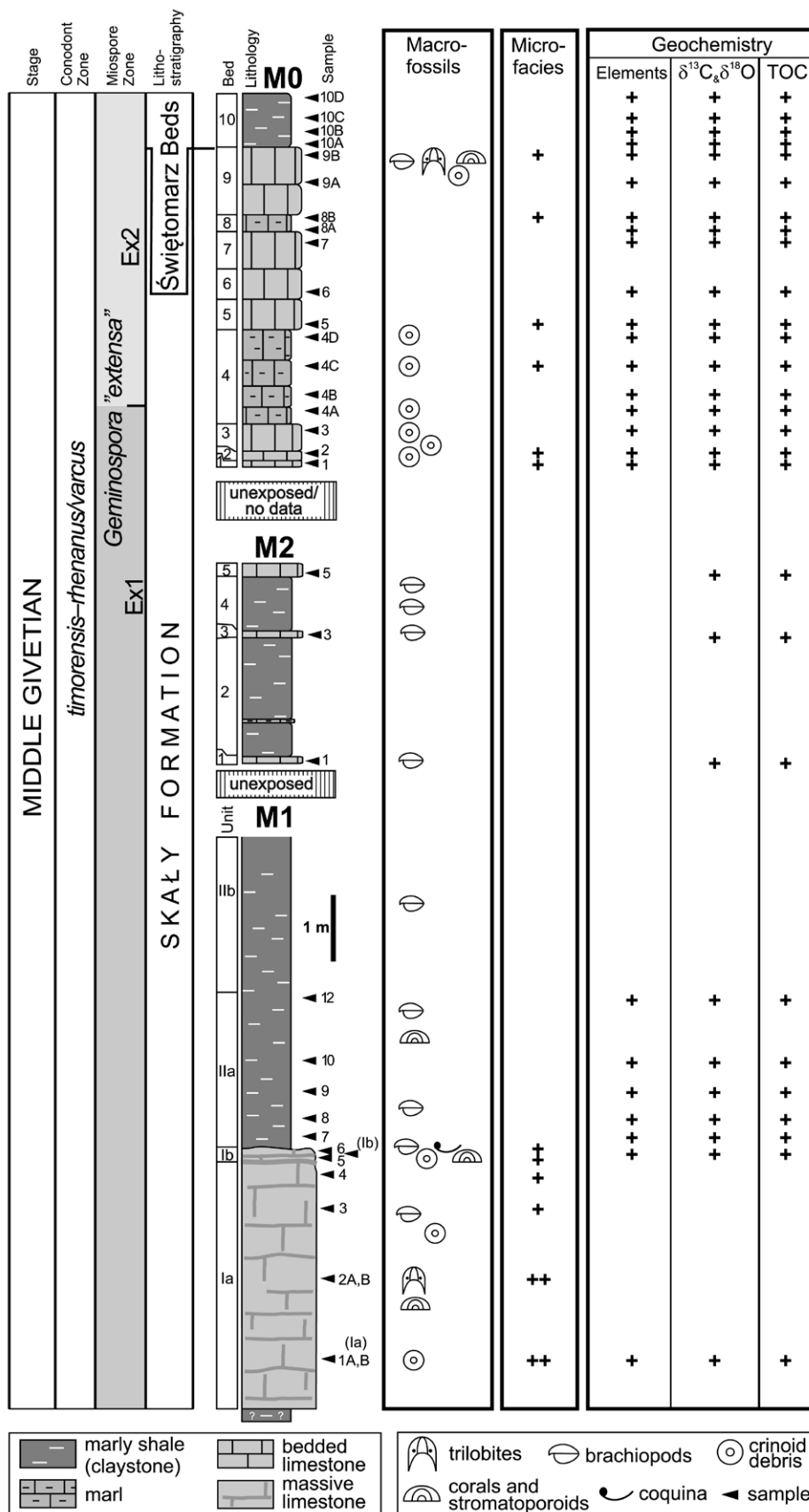


**Fig. 2.** Generalized lithology and stratigraphy (after figure 3B in Halamski *et al.*, 2022) of the Miłoszów sections (see Fig. 1C) with occurrences of macrofossils and marked samples for microfacies and geochemical (major and trace elements, carbon and oxygen isotopes, total organic carbon [TOC]) analyses. According to the local division, the Ex ("*Geminospora*" *extensa*) Miospore Zone is divided into three subzones: Ex1, Ex2 and Ex3 (Turnau, 2008). Subzones Ex1 and Ex2 were documented in the studied successions (for detailed information see Kondas and Filipiak, 2022).

the Skaly Fm in the M0 outcrop, being the hypostratotype of the upper boundary of the unit (Racki *et al.*, 2022a). The Świątomarz Beds consist of carbonate-poor shales in the basal part (see description of the unit in Malec, 2012).

In terms of conodont biostratigraphy, sections M1 and M2 represent the lower and upper parts of the *timorensis* Zone, respectively; the age of the M0 section is within the upper part of the *rhenanus/varcus* Zone (Fig. 2), even if the presence of the basal part of the *ansatus* Zone cannot be excluded (for details see Narkiewicz in Halamski *et al.*, 2022). On the basis of the miospore assemblage, the age of the deposits obtained from the M0, M1, and M2 sections were established as the Ex Zone (“*Geminospora*” *extensa*) *sensu* Turnau (1996, 2007, 2008). The index taxa for subzone Ex1 were documented in the M1 and M2 outcrops and the lower part of the M0 locality (up to sample M0-4A), where the subzone Ex1/Ex2 boundary was documented (Fig. 2; see Kondas and Filipiak, 2022). When correlated with the type area of the Skaly Fm in the nearby Dobruchna Valley, it becomes clear that the available Miłoszów sections are merely fault-controlled, small portions of a shaly-calcareous series at least 100 m thick (see fig. 9 in Halamski *et al.*, 2022).

## SAMPLES AND METHODS

Three (M0, M1, and M2) of four Miłoszów localities (Fig. 1), described in Halamski *et al.* (2022; see fig. 3; note that the numbering follows a topographic order, not that of the stratigraphic sequence), were sampled for this study. In total, 28 samples were analyzed for stable isotopes and total organic content (Fig. 2; Tab. 1), 23 were analyzed for elemental composition, and 14 limestone samples for microfacies analysis (Figs 2–4). Major and trace element concentrations were studied only in the M0 section and the marly interval (lithological set M1-IIa) in the M1 outcrop (Appendix 1), and thin sections were limited to the limestone and marly limestone of the M1 section (lithological set M1-Ia and set M1-Ib) and M0 section (see Fig. 2).

All samples range from medium to light grey in colour and (especially the limestones) are fossiliferous. Sampled rocks with CaCO<sub>3</sub> contents greater than 95% are defined as limestones and samples with 85–95% as marly limestones (see the classification of Pettijohn, 1957), both being characterized by wackestone to packstone textures. Samples with a CaCO<sub>3</sub> content in excess of 25% but not more than 85% are defined as marls (or marlstones), while CaCO<sub>3</sub>-poor samples (5–25% of CaCO<sub>3</sub>) as marly claystones (or calcareous claystones) and (< 5%) claystones. Samples with a CaCO<sub>3</sub> content of below 85% have more-or-less distinct shale-like fissility. In fact, “pure” limestones and claystones (argillaceous shales) were extremely rare in the samples studied (Tab. 1).

### Stable isotopes

The isotope compositions of carbonate and organic matter were determined for 26 samples. Powdered bulk-rock samples reacted with purified H<sub>3</sub>PO<sub>4</sub> at 70 °C. δ<sup>13</sup>C and δ<sup>18</sup>O measurements were made using a Kiel IV Carbonate

**Table 1**

Carbon and oxygen isotope ratios, CaCO<sub>3</sub> and total organic carbon (TOC) contents in the Miłoszów sections.

Carbonate content was calculated based on the formula:

$$\text{CaCO}_3 (\%) = \text{total inorganic carbon} (\%) \times 8.3333,$$

assuming that all carbonates in the sample were calcite.

Sample	δ <sup>13</sup> C <sub>carb</sub>	δ <sup>18</sup> O	δ <sup>13</sup> C <sub>org</sub>	TOC	CaCO <sub>3</sub>
	[‰]			[%]	
Miłoszów M0					
M0-10D	1.1	-3.9	-30.5	0.55	4.02
M0-10C	0.8	-4.5	-29.7	0.58	11.05
M0-10B	1.1	-4.3	-29.2	0.28	9.46
M0-10A	1.3	-4.0	-29.5	0.32	20.01
M0-9B	1.0	-3.4	-29.7	0.20	79.76
M0-9A	1.5	-4.1	-29.0	0.13	90.21
M0-8B	2.3	-4.7	-28.7	0.28	80.25
M0-8	2.0	-4.9	-29.1	0.45	74.04
M0-7	2.0	-5.1	-28.9	0.39	82.81
M0-6	1.4	-4.4	-28.4	0.15	95.40
M0-5	1.6	-3.3	-28.2	0.36	94.57
M0-4D	2.0	-4.8	-27.9	0.45	72.66
M0-4C	1.6	-3.5	-27.5	0.52	82.21
M0-4B	2.2	-5.0	-28.7	0.84	62.50
M0-4A	1.7	-5.8	-30.1	0.63	36.84
M0-3	1.8	-4.5	-27.8	0.55	92.01
M0-2	1.8	-4.3	-26.6	0.40	93.16
M0-1	1.8	-4.9	-28.3	0.38	95.21
Miłoszów M2					
M2-5	1.3	-3.2	-26.9	0.40	85.94
M2-3	0.0	-2.7	-26.8	0.32	89.91
M2-1	-2.6	-2.7	-27.4	0.81	78.89
Miłoszów M1					
M1-12	1.7	-5.4	-27.2	0.39	12.44
M1-10	2.0	-5.9	-28.1	0.50	21.60
M1-9	2.1	-6.0	-29.7	0.20	12.37
M1-8	1.8	-5.6	-29.7	0.36	13.02
M1-7	1.9	-5.8	-29.8	0.37	11.79
M1-Ib (top)	2.4	-5.6	-27.2	0.69	93.80
M1-Ia (bottom)	1.0	-4.9	-27.8	0.44	94.36

Device, connected to a Finnigan Delta Plus isotope ratio mass spectrometer. Carbon isotope measurements were made on organic matter after decarbonation of the samples; powdered samples reacted with 10% HCl for 8h at 60 °C in a water bath. Following dissolution, the residues were repeatedly rinsed with deionized water. Analyses of organic

carbon ( $\delta^{13}\text{C}_{\text{org}}$ ) isotope signatures were obtained, using a Thermo Flash EA 1112HT elemental analyser, connected to a Thermo Delta V Advantage isotope ratio mass spectrometer in a Continuous Flow system. All isotope analyses were performed at the Institute of Geological Sciences, Polish Academy of Sciences in Warsaw, Poland. Isotopic values for carbon and oxygen are reported per mil (‰), relative to the Vienna PeeDee Belemnite (VPDB) standard and calibrated using certified international standards (NBS 18, NBS 19 and IAEA-CO-9). The precision of the isotope analyses is  $\pm 0.06\text{‰}$  ( $\delta^{13}\text{C}_{\text{carb}}$ ),  $\pm 0.33\text{‰}$  ( $\delta^{13}\text{C}_{\text{org}}$ ),  $\pm 0.11\text{‰}$  ( $\delta^{18}\text{O}$ ).

### Inorganic geochemistry

The samples from Miłoszów were analyzed for major and trace element abundances at the Acme Analytical Laboratories (Vancouver) Ltd, Canada. Total concentrations of the major oxides and several minor elements were reported from a 0.2 g sample analyzed by ICP-emission spectrometry, following lithium metaborate/tetraborate fusion and dilute nitric digestion. Rare earth and refractory elements (e.g., Th, U, V, Zr) were determined by ICP mass spectrometry, following the same decomposition method. A separate 0.5 g split was digested with 3 ml 2:2:2 HCl–HNO<sub>3</sub>–H<sub>2</sub>O and analyzed by ICP MS for precious and base metals (e.g., Mo, Cu, Pb, Zn, Ni, As, Sb).

The chemostratigraphic study is based on conventional analyses of whole-rock bulk samples, which is the current research standard in sedimentary geology (see reviews in Sageman and Lyons, 2003; Tribovillard *et al.*, 2006; Calvert and Pedersen, 2007; Craigie, 2018). To compare element contents and ratios in the carbonate-dominated sediments with fluctuating siliciclastic dilution, the authors used the Al-normalization (E/Al) and enrichment factors (EF); (Tribovillard *et al.*, 2006). Enrichment factors were calculated as  $\text{EEF} = [(E/\text{Al})_{\text{sample}}]/(E/\text{Al})_{\text{PAAS}}$  and  $\text{EEF} = [(E/\text{Al})_{\text{sample}}]/(E/\text{Al})_{\text{WED}}$ , in which E represents the targeted element. Samples were normalized, using the post-Archean average shale (PAAS) compositions of Taylor and McLennan (1985; see also Tribovillard *et al.*, 2012) as well as the average limestone (WED; Wedepohl, 1970, 1971, 1991). Any relative enrichment was expressed by an  $\text{EF} > 1$ , a depletion by an  $\text{EF} < 1$ . Quoted correlation coefficients (r values) refer to the Spearman's rank correlation method.

### Total organic carbon

Total carbon (TC) and total inorganic carbon (TIC) were determined by an Eltra CS-500 IR analyser, calibrated using Eltra standards. Analytical precision and accuracy were better than  $\pm 2\%$  for TC and  $\pm 3\%$  for TIC. Total organic carbon (TOC) content was calculated by subtracting the TIC content from the total TC content. The analyses were provided at the Institute of Earth Sciences, University of Silesia in Katowice. Assuming that all carbonates were calcite, carbonate content (in %) was calculated on the basis of the following formula:  $\text{CaCO}_3 = \text{TIC} \times 8.3333$ . For more details on this established process, see Rakociński *et al.* (2021).

## MICROFACIES ANALYSIS

### Section M1

The investigated Lower Givetian limestone section M1 (units Ia and Ib; see Figure 2) consists of different microfacies types (terms after Flügel, 2010), including fine-bioclastic packstone, peloidal wackestone-packstone, stromatoporoid floatstone and coral floatstone-rudstone (Figs 3, 4D–F, and 5A, B, D–S; Tab. 2; Appendix 2). Massive limestones of the subset M1-Ia (see Halamski *et al.*, 2022) include mostly varieties of bioturbated bioclastic packstone, locally neomorphosed (samples M1-2A, M1-2B) and dolomitized (sample M1-4), and also variably red-coloured because of iron oxides (Figs 4–6). Numerous silt-sized peloids are found at some levels (samples M1-1, M1-4). In addition to substantial echinoderm debris, dominated by crinoid ossicles, abraded skeletal grains include brachiopods (as single, small shells) and molluscs (mostly gastropods?), associated with fragmented and/or abraded corals (Fig. 3C). Additionally, smooth-shelled ostracods, trilobites, and calcispheres (e.g., *Parathuramina*, *Bisphaera*, *Radiosphaera*, *?Irregularina*) frequently occur. Subordinate fossil groups include ramose stromatoporoids (amphiporoids), echinoids (spines only), microconchids, uniserial foraminifers (*Eonodosaria* and *?Tikhinella*), problematic *Rothpletzella*, and green algae (*?Litanaia*). Some bioclasts were overgrown by microbial girvanellid microstromatolites (Fig. 5E), while many crinoid elements show pervasive microendolithic borings (Fig. 5D). Bioturbation fabrics are visible not only in the comminution of skeletal elements (to grains, sized in tenths of a mm), but also in very irregular (patchy) packing densities of bioclasts, forming locally twisted structures, varying grain sorting and micrite textures, and obscure burrow structures (Fig. 3A, C).

Skeletal grains are less numerous in the burrowed peloidal wackestone-packstone (sample M1-3; Fig. 3A) and comprise fragmented tabulates and stromatoporoids, associated with debris of crinoids, trilobites, ostracods, molluscs, brachiopods and ostracods. Scattered reef-builders, embedded in partly neomorphosed fine-bioclastic micritic matrix, are enriched in stromatoporoid/coral floatstone (Figs 3D, 4F). Tabulates are exemplified by heliolitids, and massive stromatoporoids are overgrown by microbial (probably girvanellid) shrubs. The worn, large-sized bioclasts are associated with brachiopods, molluscs, crinoids, and rugose corals. The microfacies is characterized by abundant calcispheres (e.g., *Radiosphaera*, *Parathuramina*, volvocacean algae, and *?Irregularina*; Fig. 5F–H, K).

Coral-rich layers in the uppermost part of the limestone horizon (lithological set M1-Ib; see Fig. 6) represent coral floatstone/rudstone, with a bioclastic-peloidal micritic matrix and scattered micritic intraclasts. Various sized, often fragmented and abraded skeletal grains include rugose and tabulate corals, and platy stromatoporoids, paired with crinoid-shell detritus. The co-occurrence of trilobites, microconchids and rostroconchids is noteworthy. The fossil association in the intraclasts encompasses crinoids, trilobites, brachiopods, molluscs, and calcispheres.

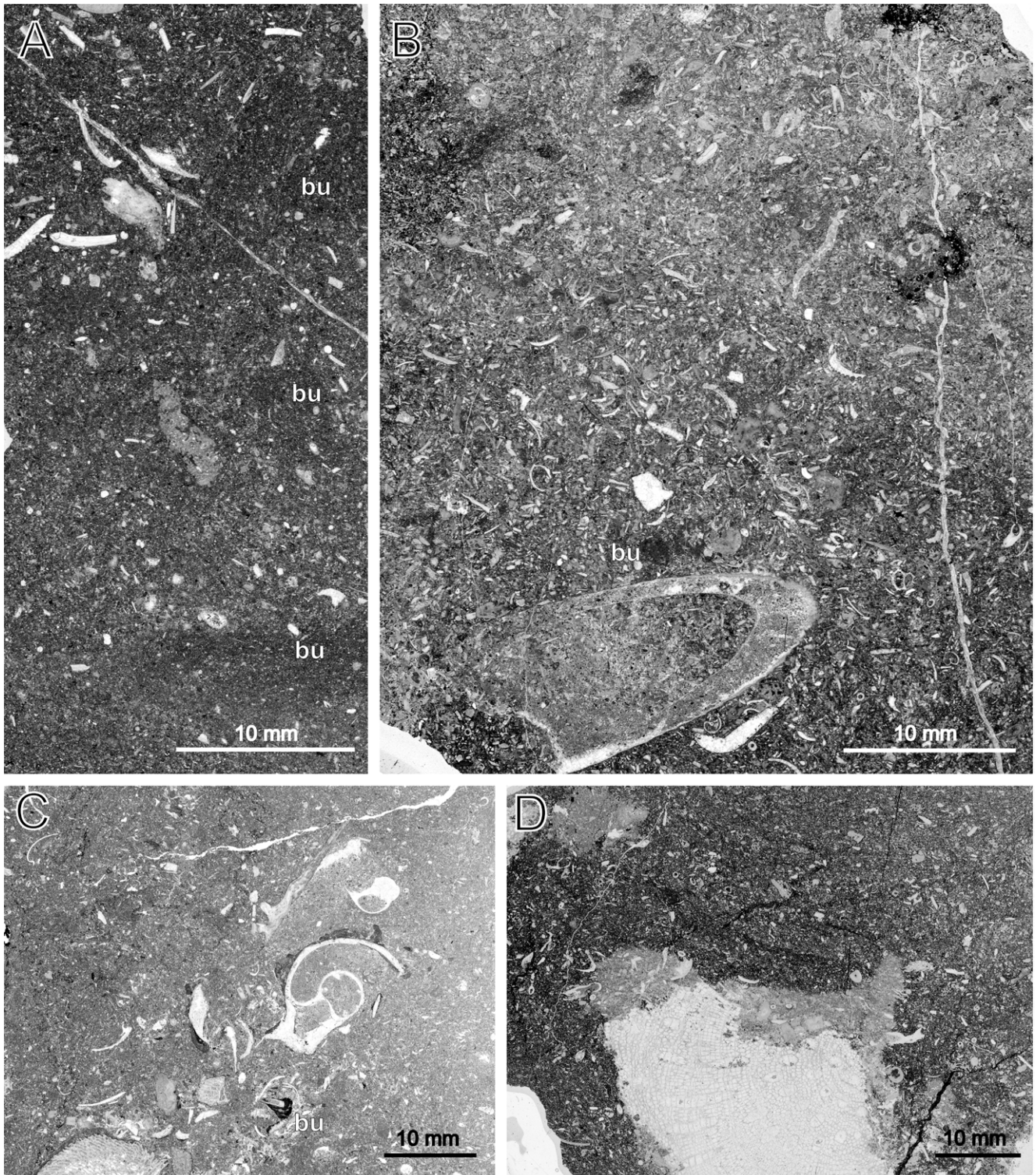


**Fig. 3.** Examples of microfacies in the Miłoszów M1 section. **A.** Burrowed peloidal wackestone-packstone (sample M1-3). **B.** Crinoid-brachiopod packstone with partly dissolved gastropod shell (sample M1-1A). **C.** Burrowed bioclastic packstone with numerous gastropods and tabulate coral (sample M1-1B; see microbial encrustation in Fig. 5E). **D.** Fine-bioclastic packstone with abraded coralliths or colony of the tabulate coral *Heliolites* (sample M1-2B). Note the indistinct burrowing structures (bu) in bioturbated heterogeneous matrix (A and C), as well as its differentiated impregnation with iron oxides (B and D).

## Section M0

The Middle Givetian outcrop M0 includes mostly macrofossil-poor limestone layers (see Halamski *et al.*, 2022), corresponding to bioclastic packstone, which passed upward into burrowed bioclastic wackestone-packstone (Fig. 4A–C; Tab. 2; Appendix 2). The muddy microfacies types are overall similar to the dominating crinoid-shell variety in the lithological set M1-I, characterized by intensively bioturbated fine-bioclastic fabrics, frequently with shell hash concentrations and microbored echinoderm detritus. Small coral clasts are more common, only in the lower interval (M0-2 to M0-4). Other skeletal grains are less diverse, represented mainly by trilobites, smooth-shelled ostracods, gastropods, amphipores, calcispheres, and echinoid spines.

An abundance of branched bryozoans and octactinellid sponge spicules characterizes samples M0-4C (Fig. 7), M0-5 and M0-9B. In the upper part of the section, the

frequency of calcispheres (e.g., *Parathuramina*) distinctly decreases, but ferruginous ?*Staneiria*-like coccoidal cyanobacteria are uniquely present (Fig. 4C). The abundance data were supplemented by microremain assemblages from macerated marly samples (Fig. 7). Note that no microfacies analysis was performed on section M2 (Fig. 2).

## GEOCHEMICAL RESULTS

A low CaCO<sub>3</sub> content (12% to 22%) occurs in the upper shaly (clayey) part of the older succession, M1 (Fig. 8). Thus, these units can be classified as marly claystone; however, it is noteworthy that their geochemical signature can be somewhat biased by near-surficial weathering.

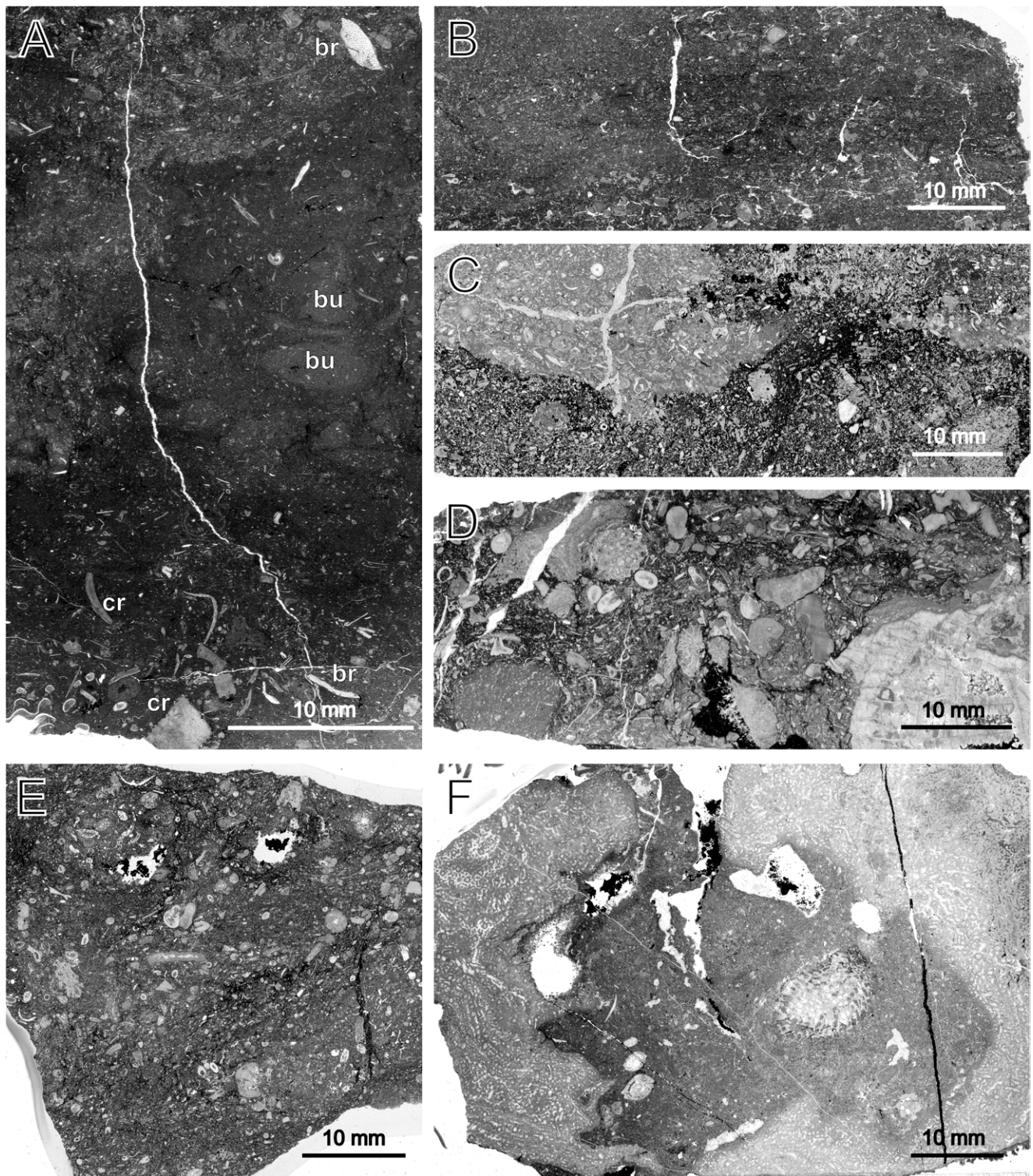
The M0 succession represents limestone-dominated (Skały Fm) and clay-rich (Świętomarz Beds) lithologies. The beds M0-1 to M0-9 of the Skały Fm are characterized by interbedded marl and limestone, with calcium carbonate

Table 2

Occurrence of particular groups of skeletal grains in the Miłoszów sections M1 and M0.

Fossils/sample	M1-1A	M1-1B	M1-2A	M1-2B	M1-3	M1-4	M1-5	M1-6	M0-1	M0-2	M0-4	M0-5	M0-8B	M0-9B
massive stromatoporoids			++		+		+							
sponge spicules											+	+		+
Rugosa corals		+	+	+			++				+			+
Tabulata corals	+	+	+	+	+	+	+	+	+	+	+	+		+
bryozoans	+					+		+	+	+	++		+	+
brachiopods	++	+	+	++	+	++	++	++	++	++	++	++	++	++
crinoids	++	+	+	+	+	++	++	++	++	++	++	++	++	++
echinoid spines	+	+						+	+				+	
gastropods	+	+							+	+		+		
mollusc shells	++	++	+		+		+	++	++	++		++	++	
smooth-shelled ostracods	+	+	+	+	+	+	+	+	+	+	+	+	+	+
trilobites	+	+			+		+	+	+		+			+
microconchids						+		+						
foraminifers	+	+							+					
amphiporoids		+				+						+		
calcispheres	+	++	+		++	++	+		++	+	+	+	+	
green algae		+				+								
girvanellid cyanobacteria		+	+			+								
Rothpletzella	+													
<i>Staneiria</i> -like cyanobacteria														+
?Microcodium													+	
Microfacies	P	P	F	P	W/P	P	F/R	P	P	P	P	P	P	W/P

Fossil frequency: ++ – numerous; + – occur. Type of microfacies: W/P – wackestone/packstone; P – packstone; P/G – packstone/grainstone; F – floatstone; F/R – floatstone/rudstone.



**Fig. 4.** Examples of microfacies in the Miłoszów M0 and M1 sections. **A.** Burrowed fine-bioclastic wackestone-packstone with accumulated crinoid remains (cr) and fragmented brachiopod valves (br) in the bottom part of graded interval; note several horizontal burrows (bu) in the middle wackestone portion (sample M0-9B). **B.** Crinoid-brachiopod packstone, distinguished by coral debris and bryozoans (sample M0-4C). **C.** Fine-bioclastic packstone with partly neomorphosed matrix containing echinoderm-shell debris, affected by iron oxide mineralization (sample M0-2). **D.** Coral floatstone-rudstone, marked by unsorted crinoid-rich matrix (sample M1-5; compare Figure 6). **E.** Crinoid packstone (sample M1-4). **F.** Stromatoporoid floatstone (sample M1-2A). Note incipient stylobrecciation, marked by iron oxides (C–E).

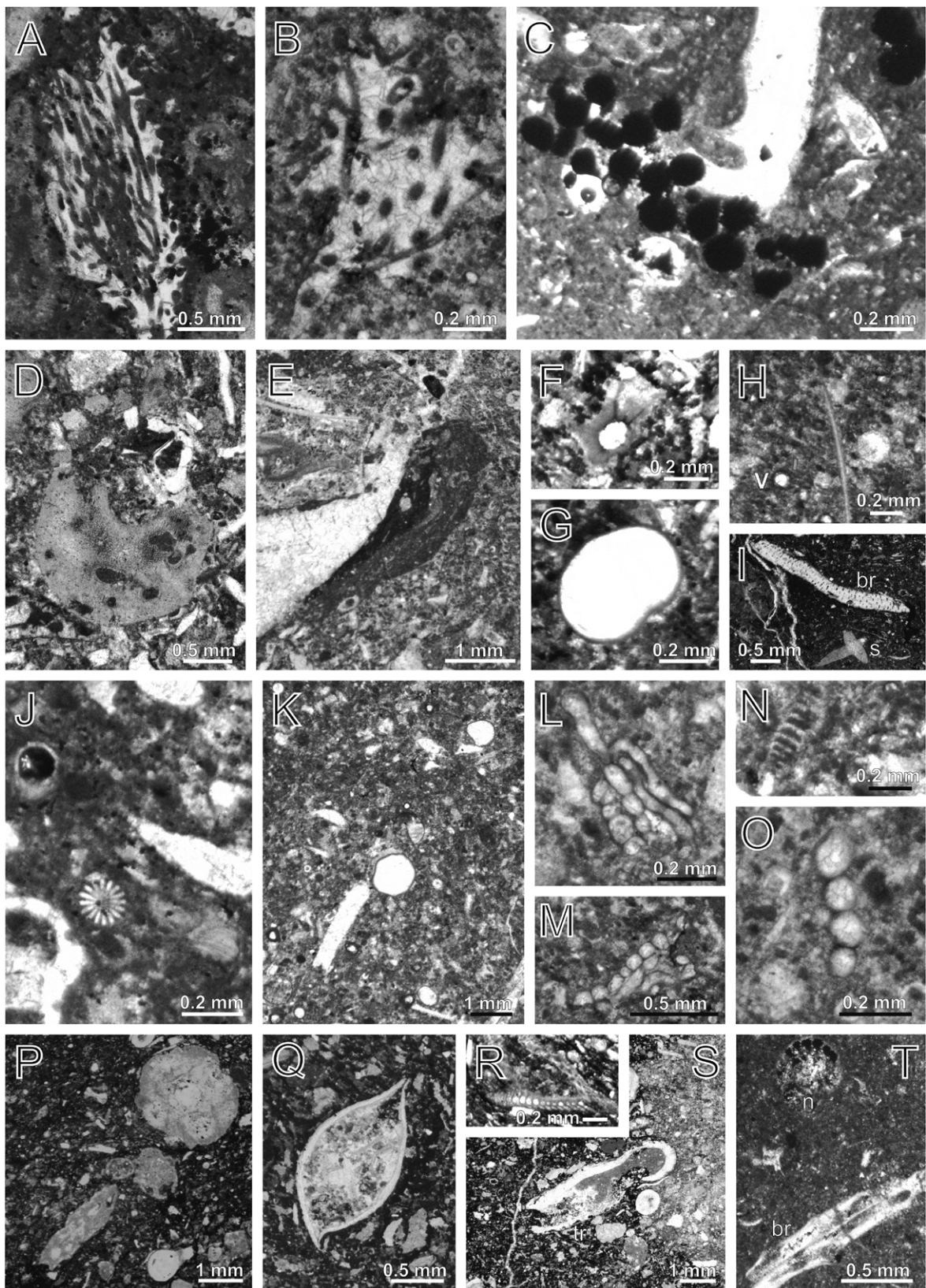


**Fig. 5.** Micropalaeontological features of the Miłoszów limestone microfacies. **A, B.** Green algae, *?Litanaia*; samples M1-4 (A) and M1-1B (B). **C.** Ferruginous *?Stanieria*-like coccoidal cyanobacteria (sample M0-9B). **D.** Microendolithic borings of crinoid columnals (sample M1-1A). **E.** Microbial crust of *Girvanella* (sample M1-1B; Fig. 3C). **F.** Calcisphere *Parathurammia* (sample M1-4), **G.** Calcisphere *Bisphaera* (sample M1-4). **H.** Radiosphaerid calcispheres and volvocean algae (V) (sample M1-3). **I.** Sponge spicule (s) and fragment of brachiopod (br) (sample M0-9B). **J.** Echinoid spine (sample M1-1A). **K.** Different varieties of calcispheres (sample M1-3). **L, M.** Problematic *Rothpletzella* (sample M1-1B). **N.** Foraminifer *?Tikhinella* (sample M1-1A). **O.** Foraminifer *Eonodosaria* (sample M1-1B). **P.** *Amphipora ramosa* (sample M1-4). **Q.** Small brachiopod (sample M1-2B). **R.** Rostroconchid (sample M1-6), **S.** Trilobite (tr) (sample M1-2B). **T.** Broken fenestrate bryozoan (br) and foraminifer *?Nanicella* (n) (sample M0/9B).

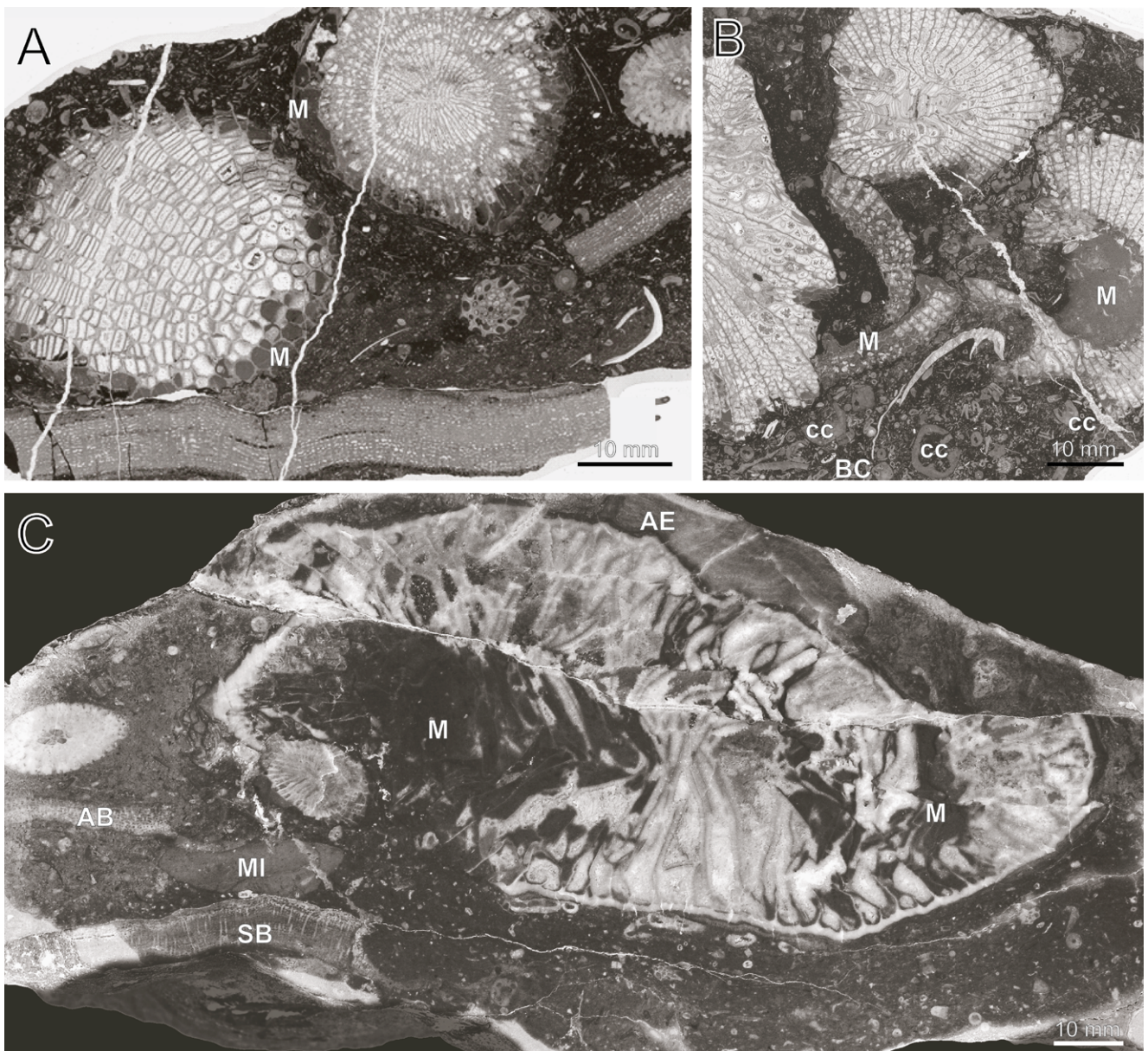


**Fig. 6.** Lithology of the coral-rich M1-I subset at the M1 locality. **A, B.** Abraded and broken coralliths and platy stromatoporoids in crinoid-brachiopod packstone matrix stained by dark brown Fe-oxides, unit M1-Ib; note coarse crinoid debris (partly bored; BC) including calyces (B – lower part, cc). **C.** Coral-intraclastic accumulation (biointrarudstone), with the large rugosan corals (cut and slightly displaced along the subhorizontal fracture) encrusted by an alveolitid (AE); fragmented lamellar stromatoporoid (SB) and alveolitid (AB), and micritic intraclast (MI) floated in crinoid-rich wackestone matrix; lithological unit M1-Ib, sample M1-5 (courtesy of Andrzej Baliński; see also Halamski *et al.*, 2022, fig. 4C). Textural inversion is indicated by infilling of outer coralith parts with pure micrite (M) and by their partial destruction during postmortem exhumation, downslope transport, and rapid allochthonous deposition.

content between 80 and 95% and the purest limestone varieties are limited to the basal part (Figs 7, 8). The main exceptions are “shale-like” intervals M0-4 and M0-8, referred to as marls (with a minimum of 37% CaCO<sub>3</sub> in sample M0-4A). In the uppermost layer, M0-10 (= basal Świętomarz Beds), the clay admixture increases and even exceeds 95% (in the topmost sample M0-10D).

#### Carbon and oxygen isotope trends

Carbonate carbon isotope data (Fig. 8) reflect fluctuations from baseline values of around 2‰ (M1 section) decreasing

to 0.0‰ (M2 section, with one-point drop to -2.6‰ values in sample M2-1), then back to 2‰ (in M0 section). A small  $\delta^{13}\text{C}_{\text{carb}}$  drop of 1.2‰ to values of around 1‰ occurs in the upper part of the M0 section, near the boundary between the Skąły Fm and the Świętomarz Beds. The carbon isotope record of organic matter ranges from -30.5 to -26.5‰ (Fig. 8). The most positive  $\delta^{13}\text{C}_{\text{org}}$  values occur in the M2 section. Two positive  $\delta^{13}\text{C}_{\text{org}}$  shifts (to values of -26.6‰ and -27.7‰, respectively), separated by a negative excursion (to -30.1‰, sample M0-4A-B), are observed in the lower part of the M0 outcrop. Thereafter, the  $\delta^{13}\text{C}_{\text{org}}$  ratios gradually decrease toward the top of the M0 section.

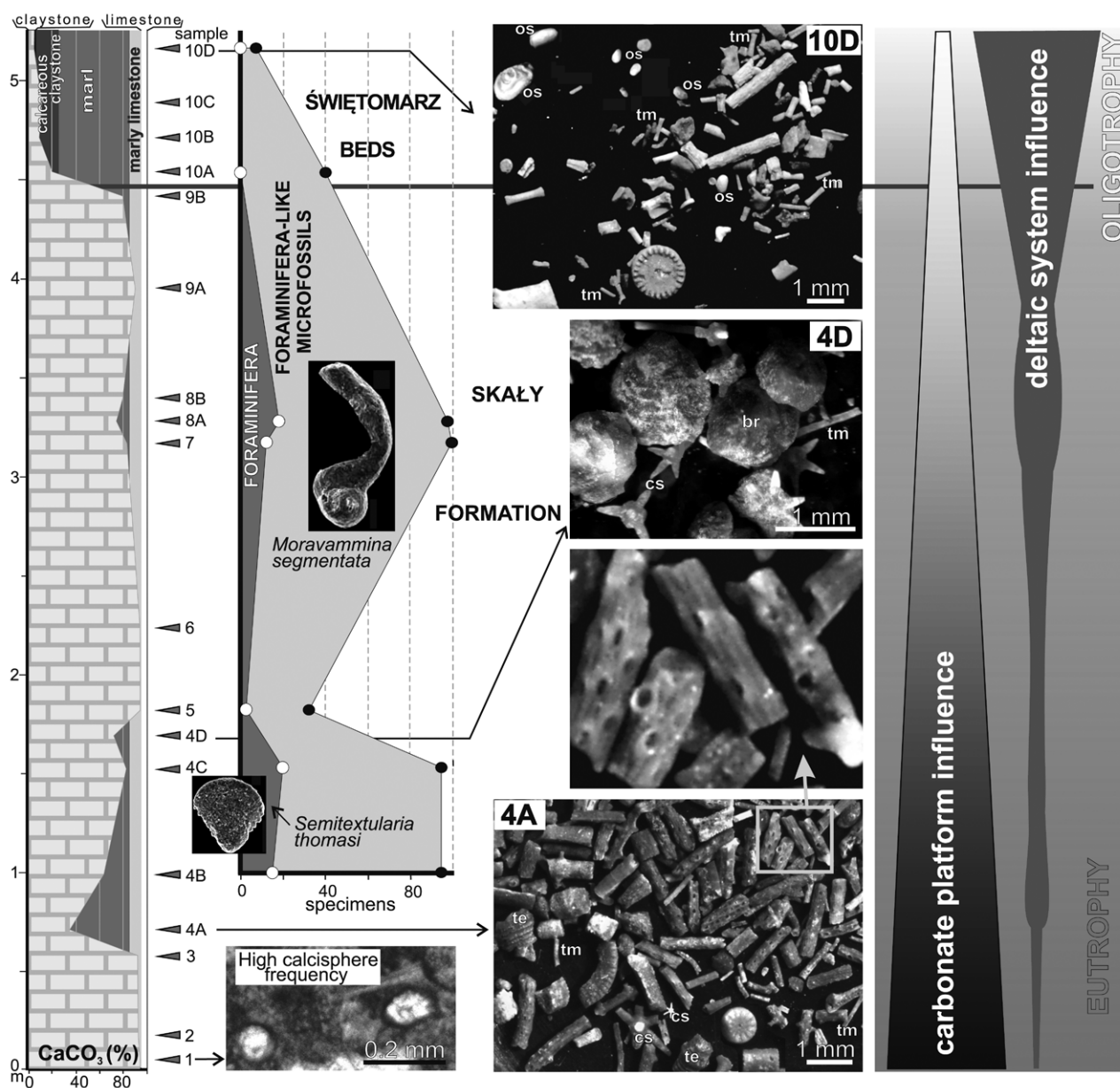


**Fig. 7.** Abundance changes of foraminifera (fig. 1 in Gajewska, 2022) and related calcareous microfossils plotted alongside the lithological changes in the M0 section, shown in terms of sedimentary control interplay in the Lysogóry carbonate ramp between the Kielce carbonate platform (exemplified also by calcisphere frequency) and prograding siliciclastic deltaic system (see Malec, 2012), recorded in the retreating open shelf biota of the Skąły Fm and of the Świętomarz Beds, respectively. Diverse marine fossil microremains from the layer M0-4 were dominated by bryozoans and crinoids [also micromorphic brachiopods, mostly *Bifida* (br), tentaculites (te), differently-sized spicules of octactinellid calcisponges (cs), and tubular microproblematics (tm; compare Form D in Gajewska, 2022)], while impoverished association in the layer M0-10 is distinguished by abundance of ostracods (os).

The oxygen isotope values in the M1 section range from -5‰ to -6‰ (Fig. 8). An increase of  $\delta^{18}\text{O}$  values to -3‰ occurs in the M2 section.  $\delta^{18}\text{O}$  values vary from -6‰ to -3‰ in the M0 outcrop.

#### Elemental composition

The geochemical data presented (Fig. 9) highlight elemental concentrations and proxies that aid the interpretation of the depositional environment of the Miłoszów sections, including major oxides ( $\text{SiO}_2$ ,  $\text{Al}_2\text{O}_3$ ,  $\text{TiO}_2$ ,  $\text{K}_2\text{O}$ ,  $\text{Na}_2\text{O}$ ,  $\text{Fe}_2\text{O}_3$ ,  $\text{CaO}$ , and  $\text{MgO}$ ), trace elements (e.g., Zr, Th,

U, Mo, Cd, Zn and V), and total organic carbon. A geochemical dataset is available in the supplementary data (Appendix 1).

Information on oceanic palaeoproductivity and proximity to coastlines can be obtained by determining the source of silica in the samples (Fraser and Hutchison, 2017). A silica source can be inferred from its relationship with zirconium (Zr), an element typically used as a proxy for terrestrial input (e.g., Wright *et al.*, 2010; Blood *et al.*, 2013; Hall *et al.*, 2013). The high  $\text{SiO}_2/\text{Zr}$  ratios indicate biogenic silica enrichment. The element Al is most commonly utilized as the primary indicator of fine-grained detritus, and the Si/Al

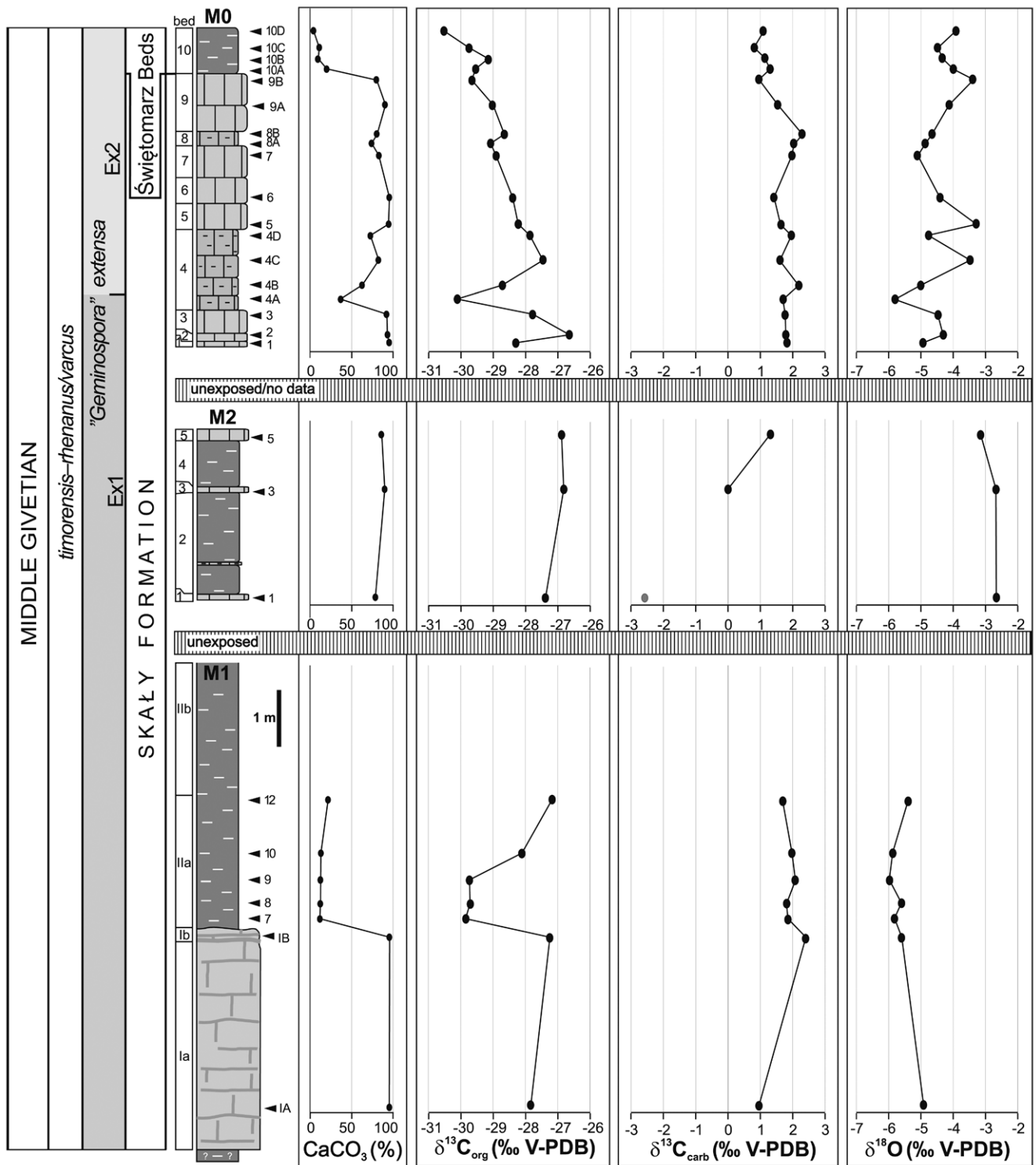


**Fig. 8.** Carbon and oxygen isotope and  $\text{CaCO}_3$  records in the Miłoszów sections. One-point  $\delta^{13}\text{C}_{\text{carb}}$  drop (grey point) at the M2 section is interpreted as diagenetic overprinted.

ratio as a proxy for sand-dominated ( $> 5$ ) or clay ( $< 5$ ) lithologies (see Ver Straeten *et al.*, 2011). Thorium (Th), Hf, and Zr concentrations (positively correlated with detrital clay volume; Ratcliffe *et al.*, 2012) and terrigenous input profile (TIP; Hildred and Rice, 2014; Pyle and Gal, 2016) were used to determine the terrigenous input. The TIP is the summed weight percent of  $\text{Al}_2\text{O}_3$ ,  $\text{TiO}_2$ ,  $\text{K}_2\text{O}$ , and  $\text{Na}_2\text{O}$ , oxides that are almost entirely related to land-derived sediment and may be immobile during diagenesis (Tribovillard *et al.*, 2006).

The products of enhanced chemical weathering generally have higher Rb and Cs concentrations than the parent rocks (Yan *et al.*, 2007). While Al, Ti, Th, Hf, and Zr are relatively resistant to chemical weathering (Tylor and McLennan, 1985). Hence, Rb/Th and Cs/Ti ratios can provide evidence of chemical weathering intensity and indirect evidence of climatic conditions (Yan *et al.*, 2007).

Redox-sensitive trace metals, such as Mo, U, As, Co, and Sb, have been used to reconstruct palaeocean chemistry

(Tribovillard *et al.*, 2006; Algeo and Maynard, 2008). In strata under lower dysoxic to anoxic conditions, these elements bond to organic matter or form sulphide compounds. Therefore, a strong positive covariance between the concentrations of U, V, Mo, and U and the accumulation of TOC was found by many researchers under anoxic conditions (e.g., Sageman and Lyons, 2003; Algeo and Lyons, 2006). Enrichment in molybdenum also takes place under oxic conditions, but Mo is scavenged mainly by Mn and Fe oxyhydroxides. Among potentially autogenic elements, Mo and U are considered to be indicators of redox states, while Cd and Zn are seen as nutrient proxies (Tribovillard *et al.*, 2006).

Covariation patterns show two distinctive groups of elements (Appendix 1): (1) related to the detrital clay fraction, that is, controlled by detrital input ( $r_s > 0.9$  with Al; most elements, such as Al, Si, Zr, Ti, K, and Na, but also Ba, Mg, Ni, Cu, Co, and V, among others), and (2) unrelated to the clay fraction, that is, at least partly of autogenic origin. An independent position is taken by Zn (lack of any compatibility with other elements, excluding U and Cd), while U has a generally weak correlation with the siliciclastic tracers.

The  $\text{SiO}_2$  contribution is highly variable, from ~2% to 47%. All lithologies show similar TOC contents, ranging from 0.13 to 0.94 wt. % (Fig. 9; Tab. 1). Only a few elements (U, Zn, and Cd) exhibit a moderate positive correlation with TOC ( $r_s$  around 0.5,  $p < 0.05$ ; Appendix 1). Strong positive correlation occurs between Mo and Mn ( $r_s = 0.77$ ,  $p < 0.05$ ). Mo, U, As, and Sb enrichment factor curves at Miłoszów sections are similar, although absolute values vary considerably, with the order of enrichment of all samples, relative to an average shale, as follows:  $\text{As} > \text{U} > \text{Mo} > \text{Sb}$ . The Th/U ratio, commonly used as the palaeoredox proxy (Tribovillard *et al.*, 2006; Rakociński *et al.*, 2021), shows a pattern similar to the land-derived elements (such as Th and Zr; Fig. 9).

When compared with the average limestone, as defined by Wedepohl (1970, 1971, 1991), the limestone samples from Miłoszów display negligible differences, exemplified by some enrichment in Zn, as well as Nb, La, and Y (Appendix 1). Dolomitization remains unimportant in the studied samples, as the MgO content is on average 1% and linked with aluminosilicates ( $r_s = 0.93$  with Al).

## IMPLICATIONS FROM CARBON AND OXYGEN ISOTOPE RECORDS

Previous stable carbon and oxygen isotope data come from foraminifera tests (*Semitextularia thomasi*) and bulk-rock samples from Miłoszów (Fig. 10) and Skały sections (Dubicka *et al.*, 2021; Gajewska, 2022). Yans *et al.* (2007) measured  $\delta^{13}\text{C}_{\text{carb}}$  in scattered brachiopod calcites from the lower part of the Skały Fm at Skały, and obtained a value of 3.1‰ in the highest sample from the Lower *varcus* (= ?*timorensis*) conodont Zone (Fig. 10). The  $\delta^{13}\text{C}$  data from a marly intercalation in the Miłoszów coral biostrome of the M1-IIa unit (−0.1‰, −2.2‰; Dubicka *et al.*, 2021) are more similar to values obtained from bulk-rock samples in the M2 section (0.0‰, −2.6‰) than in our M1-7 sample (1.9‰). The samples from M1, M2, and M0

outcrops show  $\delta^{13}\text{C}_{\text{carb}}$  values more similar to the average carbon isotope values from Upper Eifelian ‘brachiopod shales’ at Skały 11 section (1.7‰; Dubicka *et al.*, 2021). The reported isotope ratios also agree with the results of Yans *et al.* (2007) from the Eifelian–Givetian transition that increase from 1.3‰ to 2.8‰, at least partly corresponding to the Kačák positive excursion, so clearly recorded in the Ardennes (Yans *et al.*, 2007, fig. 2m).

The Skały Formation represents an open-marine, outer to middle carbonate ramp facies (Halamski *et al.*, 2022; see below). Buggisch and Joachimski (2006) stated that baseline  $\delta^{13}\text{C}_{\text{carb}}$  values are between 1‰ and 2‰ in Devonian lower slope facies. The  $\delta^{13}\text{C}$  data of well-preserved brachiopod shells from upper part of the *hemiansatus* to *rhenana/varcus* zones is in the range 1.2‰ to 2.7‰ (van Geldern *et al.*, 2006). These values are not correlated with a positive offset and global events (van Geldern *et al.*, 2006, fig. 8). Most  $\delta^{13}\text{C}$  results at Miłoszów fall within the range reported for the Givetian brachiopods and lower slope settings. Only two samples from the M2 section show distinctly lower values ( $\leq 0.0\%$ ). Buggisch and Joachimski (2006) observed positive carbon isotope excursions in the Lower–Middle Givetian carbonate samples from Montagne Noire and the Rhenish Massif (~2‰), and in their opinion, the  $\delta^{13}\text{C}_{\text{carb}}$  increases coincide with the *pumilio* events. A similar  $\delta^{13}\text{C}$  pattern, based on brachiopod calcite, was found in the Ardennes in the upper *hemiansatus* – *rhenana/varcus* zonal interval (fig. 2 in Yans *et al.*, 2007; Fig. 10). The carbonate carbon isotope record at Miłoszów (as in Hühnertal, Harz, Germany; Fig. 10) in the *timorensis*–*rhenana/varcus* zones (formerly the Lower *varcus* Zone) shows several fluctuations (in magnitude ~1.5‰) but without a distinct positive excursion.

The  $\delta^{13}\text{C}_{\text{org}}$  values observed in the Miłoszów sections are within the range of data, reported from the Middle and Late Givetian marine basin that connected the Appalachian Foreland Basin with the Michigan Basin in Ontario, Canada, by van Hengstum and Gröcke (2008; revised dating in Brett *et al.*, 2011). However, the  $\delta^{13}\text{C}_{\text{org}}$  data (−30‰ to −27‰) obtained for the Miłoszów limestones are generally similar to, or slightly higher than results published for the Canadian part of Laurussia (−29.5‰ to −27.5‰ of the Hamilton Group, Ontario, van Hengstum and Gröcke, 2008; −30‰ to −28‰ of the Canol Fm, Richardson Mountains, Yukon, Fraser and Hutchison, 2017; −31‰ to −29‰ of the Prohibition Creek Member, Horn River Group, Northwest Territories, Kabanov *et al.*, 2022). Positive  $\delta^{13}\text{C}_{\text{org}}$  excursions were explained by Kabanov *et al.* (2022) as an enrichment in  $^{13}\text{C}$ , associated with an influx of isotopically heavy plant detritus. An increase in the quantities of in terrestrial spores was detected during the Late Silurian positive carbon isotope excursion, while abundant and diverse acritarch communities correlate with low stable isotope values (Stricanne *et al.*, 2006). A similar relationship between changes in marine and terrestrial palynomorph assemblages and  $\delta^{13}\text{C}_{\text{org}}$  curve deviations can be observed in the studied sections. In particular, a decrease in  $\delta^{13}\text{C}_{\text{org}}$  in the upper part of the M0 section could indicate decreasing input of terrestrial origin organic matter or an increase in the contribution of  $^{12}\text{C}$ -rich marine organic carbon.

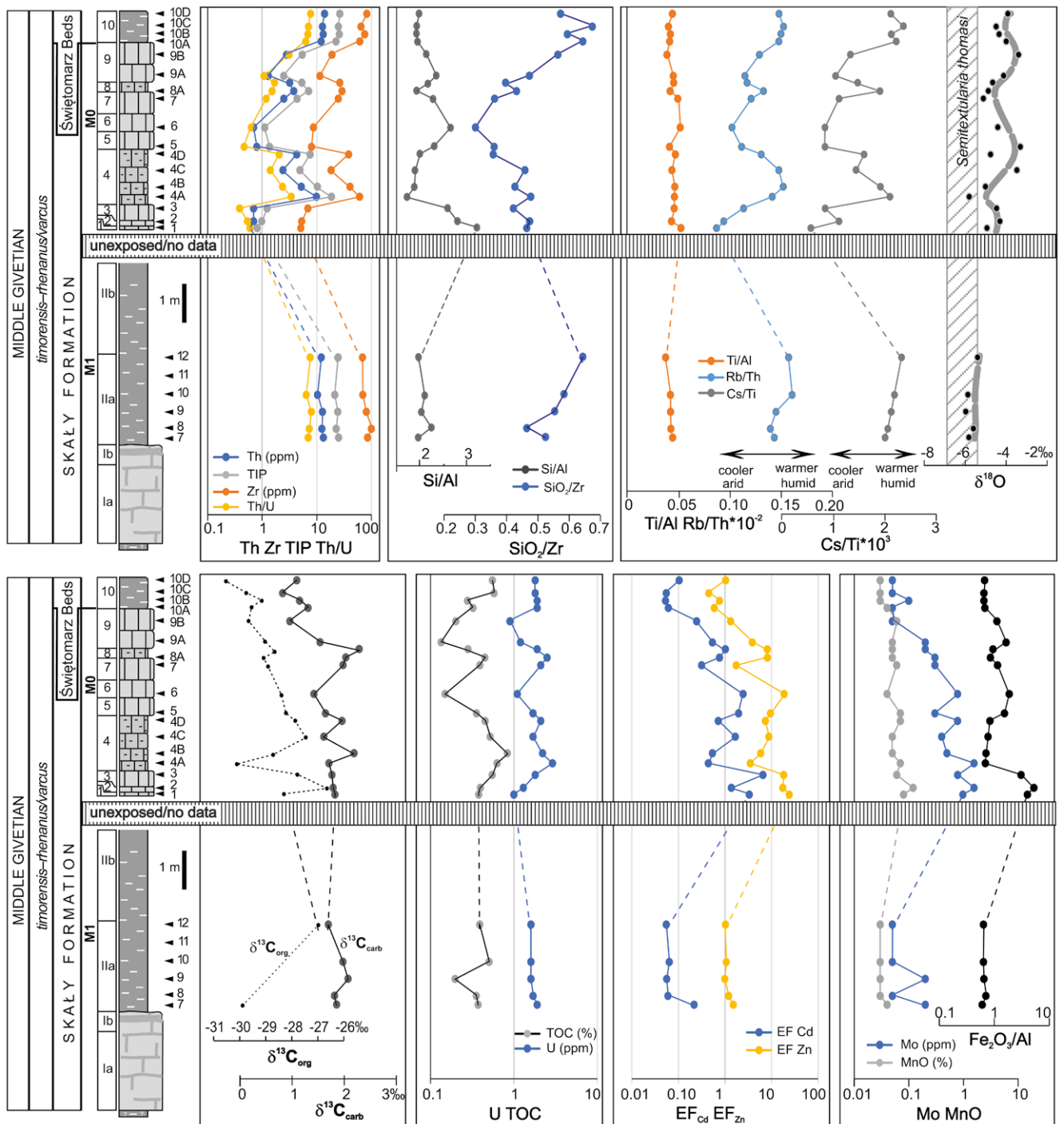


**Fig. 9.** Geochemical proxies of terrestrial input, redox condition, chemical weathering intensity, productivity and hydrothermal activity from the M1 and M0 sections (see text). Correlation of the M1 and M0 outcrops with the succession of the Grzegorzowice-Skały indicates that M0 is located about 80 m above M1 (compare to figure 8 in Halamski *et al.*, 2022). Oxygen isotope data for foraminifera *Semitextularia thomasi* from Dubicka *et al.* (2021).

Values for  $\delta^{18}\text{O}$  of the studied bulk-rock samples are similar to or higher than the  $\delta^{18}\text{O}$  data from rock and well-preserved microfossil samples from shaly lithologies in the Skały section. Averaged  $\delta^{18}\text{O}_{\text{carb}}$  values obtained by Dubicka *et al.* (2021) in the Miłoszów section (-6.4 to -6.9‰; Fig. 9) are significantly lower than the present data (-6.0 to -2.7‰; Fig. 9). Fluctuation in oxygen isotope ratios can be induced by diagenetic alterations or primary changes in seawater

salinity or/and temperature (Song *et al.*, 2019). The relatively homogeneous  $\delta^{18}\text{O}$  values in the samples from the M1 and M2 sections may be explained by the diagenetic stabilization of carbonate mud in meteoric solutions (Allan and Matthews, 1982). In this case, the oxygen isotope composition of the carbonates will be strongly related to the composition of meteoric solutions (see Joachimski, 1994). Alternatively, brachiopod calcite  $\delta^{18}\text{O}$  records during the

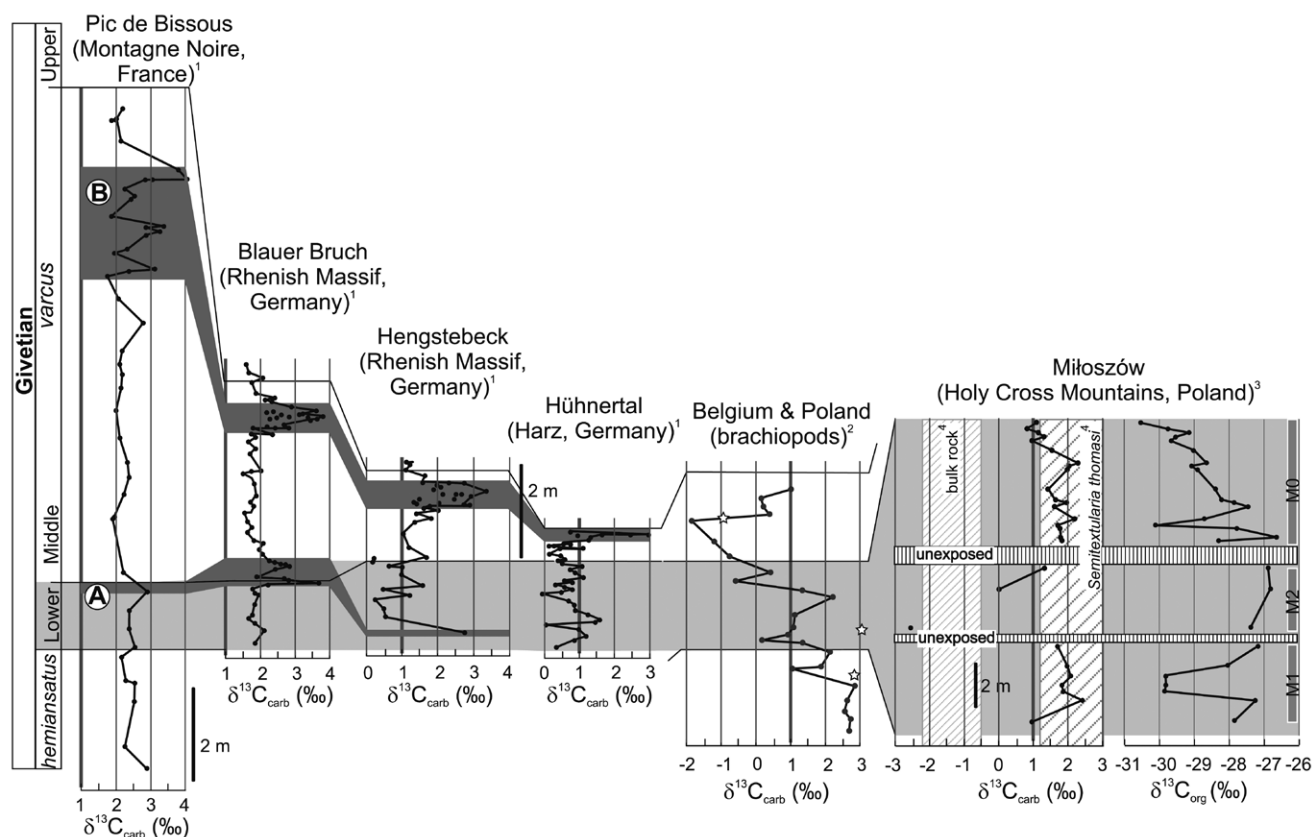


**Fig. 10.** Carbon isotope records of the Lower–Middle Givetian boundary interval, based on carbonate samples (limestones and brachiopod calcites) from Western Europe (Montagne Noire, Rhenish Massif, Harz, Ardennes) and Holy Cross Mountains. Dark grey shaded bars highlight major excursions (A – lower *pumilio* event, B – upper *pumilio* event) after Buggisch and Joachimski (2006), light grey bar – Lower *varcus* conodont Zone. 1 – Buggisch and Joachimski (2006); 2 – Yans *et al.* (2007), no thickness scale, 3 – this study, 4 – Dubicka *et al.* (2021). Asterisks indicate the  $\delta^{13}\text{C}_{\text{brachiopod}}$  values from the Skaly Fm. The relative position of data from the M1, M2, and M0 sections on the right. No thickness scale for the unexposed intervals.

*timorensis-rhenana/varcus* zones (Veizer *et al.*, 1999; van Geldern *et al.*, 2006) reflect a similar scatter of isotope ratios to those at the Miłoszów localities. This oxygen isotope record shows an extremely high  $\delta^{18}\text{O}_{\text{carb}}$  value of  $-2.9\text{‰}$  for the Middle Devonian and an increase of the conodont  $\delta^{18}\text{O}$  values during the Early Devonian to a Middle Devonian maximum ( $\sim 19.3\text{‰}$  VSMOW; Grossman and Joachimski, 2022). Interestingly, although the bulk rock  $\delta^{18}\text{O}$  values in the Miłoszów samples were most likely diagenetically altered because the  $\delta^{18}\text{O}_{\text{carb}}$  of micrites is more susceptible to diagenetic overprinting than are the brachiopods and biophosphates (see strong and moderate negative correlation between  $\delta^{18}\text{O}$  and  $\delta^{13}\text{C}$  data in the M1 and M0 sections, respectively; Appendix 3), the relatively high  $\delta^{18}\text{O}_{\text{carb}}$  values, corresponding to well-preserved brachiopod shells, indicate a surprisingly low resetting of oxygen isotopes in the analyzed calcite material (Fig. 8; see below). Further  $\delta^{18}\text{O}$  investigations (e.g., in biogenic low-Mg calcite; see Brand *et al.*, 2012, or in conodonts; Barham *et al.*, 2012) will determine whether the oxygen isotope data of whole rock samples in the Miłoszów sections reflect sea-water temperature fluctuations.

## INTERPRETATION OF ELEMENTAL PROXIES

### Silica source and terrestrial input

The Si/Al ratio ranges from 1.7 to 3.2 and indicates inflow to the basin of mainly the clay fraction (Fig. 9). The  $\text{SiO}_2/\text{Zr}$  ratio in the Skaly Fm is low ( $\leq 0.5$ ). The highest ratios ( $\geq 0.6$ ) occur in the early intervals of the M1 and M0 sections (from samples 9B to 10D). The samples from the middle part of the M0 section (samples 4D to 7) have the lowest values in the sections ( $< 0.4$ ). A  $\text{SiO}_2$  versus Zr cross-plot displays positively covarying relationships ( $r_s = 0.98$ ,  $p < 0.05$ ), indicating exclusively terrestrial-derived silica (e.g., Wright *et al.*, 2010; Pyle and Gal, 2016). The Th, TIP, Hf, and Zr trends are also lithology-related (Fig. 9) because they reveal similar patterns at the Miłoszów sections, with high values in the clay-rich M1 section and three decreasing–increasing cycles in the M0 section. The highest TIP, Th, Hf, and Zr values in the M0 section occur in the early intervals (M1-7 to M1-12; M0-4A to M0-4D; and M0-10A to M0-10D). Such proxy fluctuations can be caused by sea-level or climatic changes (Blood *et al.*, 2013; Fraser and Hutchison, 2017; see below).

### Redox conditions and bioproductivity

As described above, most of the potentially redox-sensitive elements, except for Mo and U, show strong positive correlations with elements of detrital origin (see Appendix 1). The redox-sensitive elements show distinctly decreasing values upward in the Miłoszów sections. Negligible Mo enrichment occurs only in the lower part of the M0 section. However, the lack of significant correlation between Mo and TOC contents, in contrast to the good covariation between Mo and Mn, especially for limestone samples, indicates the absorption of Mo onto Mn-oxyhydroxides during oxidative precipitation. Higher TOC values (0.4–0.8%),  $EF_{Cd}$  and  $EF_{Zn}$  in the carbonate lithologies of the Skały Fm (Fig. 9), indicate strong periods of increased productivity without drastic changes in redox states. In the M0 section, fluctuation in  $\delta^{13}C_{org}$  corresponds to chemostratigraphic trends of Zn and Cd enrichment factors. This correlation may be related to local nutrient input and the development of conditions conducive to the blooming of marine biota. Conversely, the claystone layers M1-7 to M1-12 and M0-10 are not enriched in the bio-sensitive elements. These intervals are interpretable as having been deposited in oxic oligotrophic conditions, which for the most part agrees with impoverished fossil content upward in both successions (see below).

### Weathering and climatic setting in sediment source area

A pre-Taghanic shallowing was detected in the conodont biofacies and lithology in North America (Taghanic type region in the Appalachian Basin, Nevada, and Northwest Territories of Canada), in Europe (Germany, Armorican Massif, southern France, Poland, and Carnic Alps), North Africa (Morocco), on the Siberian Craton, and in South China (summary in Aboussalam and Becker, 2011). The eustatic regression forms the uppermost part of Depophase If of Johnson *et al.* (1985), but a more complex pattern of fluctuating sea-level is proposed by Brett *et al.* (2011; Fig. 11D). On the basis of the oxygen isotope composition of biogenic apatite and brachiopod shells, Joachimski *et al.* (2009) calculated seawater temperatures of around 23 to 25 °C for the Middle Devonian, and a cooling trend from late Emsian to middle Givetian (see also Brett *et al.*, 2020). The latest data exhibit similar temperature trends for Late Ordovician to Devonian low-latitude SSTs, although Grossman and Joachimski (2022) calculate values in the range of 32–40 °C (Fig. 11E).

Climate/weathering elemental proxies (Ti/Al, Rb/Th, Cs/Ti; Kiipli *et al.*, 2012; Yan *et al.*, 2007; see also summary in Racki *et al.*, 2022b) were tested for the Miłoszów M0 and M1 successions. The Ti/Al ratios are nearly constant, indicating similar behaviour during weathering. Lower  $CaCO_3$  contents, higher Rb/Th and Cs/Ti ratios and elevated terrigenous input in the marly and claystone units (Figs 8, 9) can indicate more intensive chemical weathering in a warm and humid climate (compare Yan *et al.*, 2007). However, this tentative conclusion should be supported by the evidence from oxygen isotopes in biogenic apatite.

### Volcanic/hydrothermal processes

The Middle Givetian (Lower *varcus* conodont Zone) extensive synsedimentary alkali-basaltic volcanism is documented in the form of the lapilli-limestone-tuffite succession in the Rhenish Massif (Lahn and Dill Syncline; Königshof *et al.*, 2010). While volcanic quiescence is implied from the geochemical data under study (at the most 10 ppb in the case of Hg, Appendix 1), the interpretation of hydrothermal signatures is more complex because of probable superposition of syndepositional and post-depositional signatures in the recurrently tectonically active zone of the Holy Cross Fracture (Czarnocki, 1957; Narkiewicz *et al.*, 2006; Konon, 2007). The late Variscan metallogenesis is manifested by the nearby pyrite-siderite-hematite ore at Rudki, near Nowa Słupia, in the Łysogóry Fault zone (Rubinowski, 1969; Fig. 1B). The secondary hematitization of the limestones, referred to as hydrothermal alteration in tectonically sheared zones, is clearly visible at the top of M1-I lithological unit and variably manifested in many sectioned samples (Figs 3–4 and 6). Despite this uncertainty in the faulted Miłoszów area (Fig. 1C), both proxies applied,  $Fe_2O_3/Al$  (to limit a strong association with terrigenous input) and MnO, show the same chemostratigraphic trend of decreasing hydrothermal fluid flow (Fig. 9; see e.g., Lim *et al.*, 2020; Racki *et al.*, 2022b), interpreted as a primary feature, most likely influencing both redox and life conditions (see e.g., ferruginous coccoidal cyanobacteria in Fig. 5C).

## CARBONATE RAMP MODEL AND ENVIRONMENTAL ACCOUNT

The microfacies types of the Miłoszów limestones (Figs 3–5), combined with geochemical proxies (Figs 8, 9), characterize the middle and outer facies belt of the Łysogóry carbonate ramp (see Halamski *et al.*, 2022; Fig. 12), and may be correlated with the common ramp lithologies (RMFs), established by Flügel (2010, box 14.6, fig. 14.30). This depositional system was determined by a low-gradient slope and the facies belts passed gradually offshore into deeper-water, low-energy deposits. Although fine-grained, often burrowed, fossiliferous limestones and marls are generally referable to the outer ramp zone (i.e., below the normal storm wave base; “standard” ramp microfacies RMF 3); strongly reworked skeletal debris is considered more typical for mid-ramp settings (RMF 7 and RMF 8). However, evidence of storm-controlled sedimentation (e.g., graded distal tempestites) is rarely preserved (see Fig. 4A), which indicates a more deep-shelf quiescent muddy setting, with skeletal material disarticulated primarily by the intense activity of soft-bodied infauna. The mechanical efficiency of soft-bodied deposit feeders is evidenced in homogenized, finely comminuted bioclastic concentrations (Figs 3B, D, 4B–C). Primary sediment fabrics and individual burrows are, therefore, only sporadically recognizable.

Conversely, sparry microfacies are not found, and therefore, winnowing action, if any, was possibly compensated by *in situ* mud production by microborers. The main exceptions are breccia-like coral layers from the M1-Ib

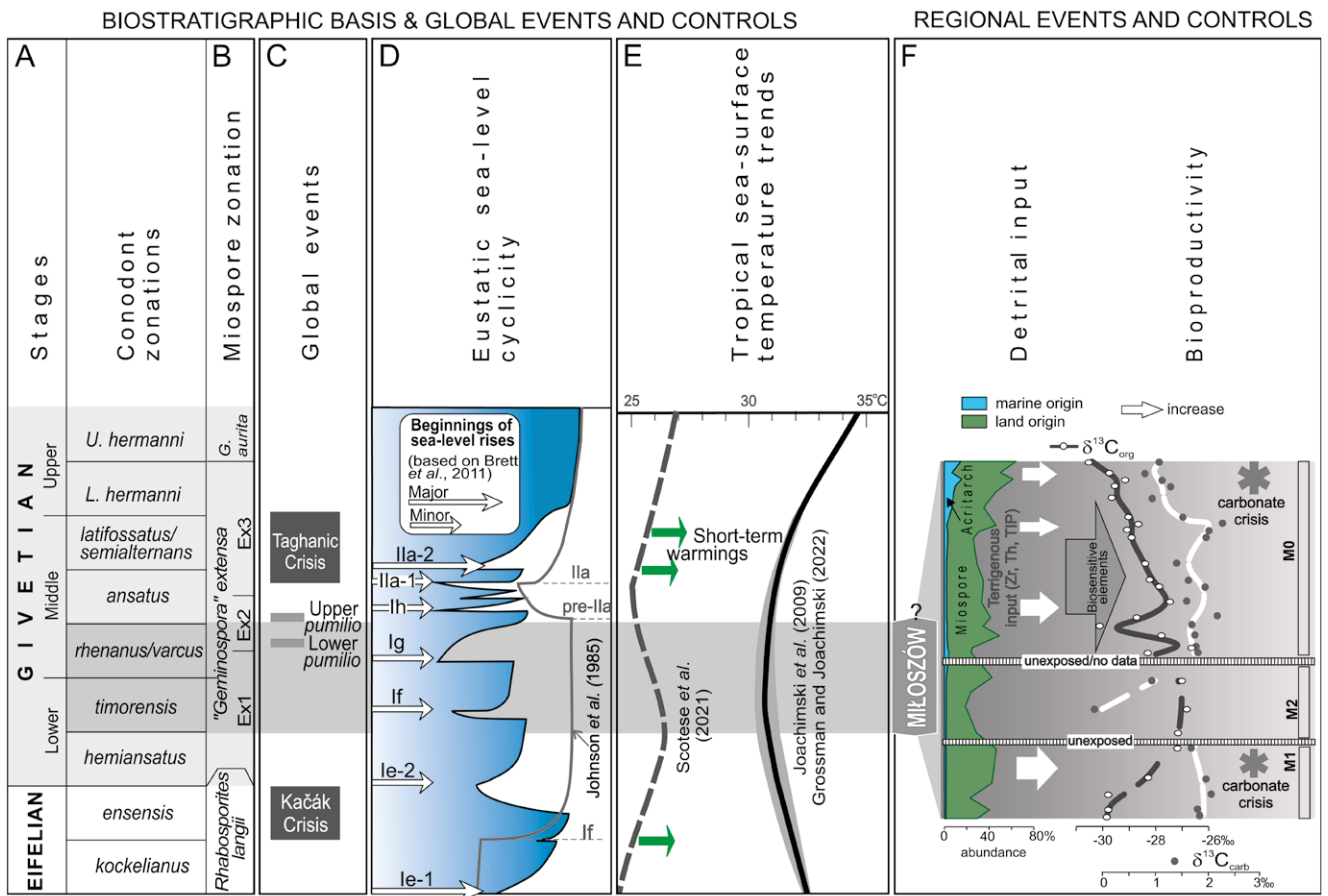


**Fig. 11.** Regional events during the deposition of the Skaly Fm at Miłoszów, against the biostratigraphic framework (Narkiewicz and Königshof, 2018; Kondas and Filipiak, 2022) and global event setting (see Halamski *et al.*, 2022, fig. 7 therein). **A.** Conodont zonation. **B.** Miospore zonation. **C–E.** Global event stratigraphy (Becker *et al.*, 2016, 2020), and eustatic (“standard” sea-level curve of Johnson *et al.*, 1985, changed by Brett *et al.*, 2011 and Brett, e-mail comm., 2022) and climatic records (Joachimski *et al.*, 2009; Scotese *et al.*, 2021; Grossman and Joachimski, 2022; Brett, e-mail comm., 2022). **F.** Regional environmental changes in the Łysogóry carbonate ramp facies. For detailed information see Halamski *et al.* (2022). No thickness scale for the unexposed intervals.

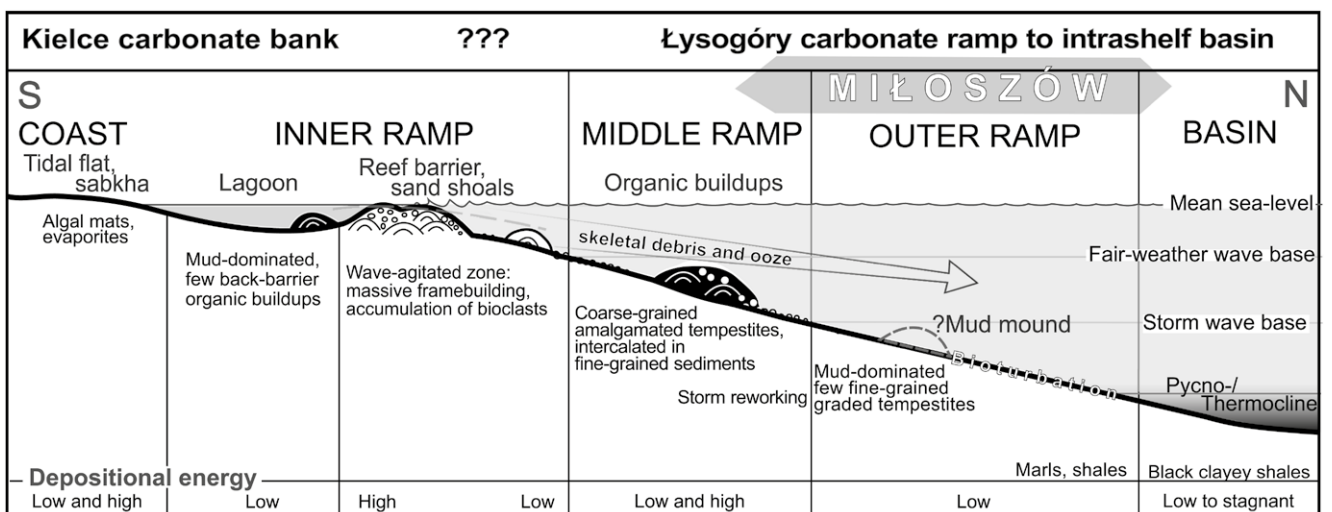


**Fig. 12.** The generalized framework of the carbonate ramp system (based on Flügel, 2010, figs 2.7 and 14.3, and box 2.4), adapted to the Holy Cross shelf domain by highlighting a depositional role of stromatoporoid-coral skeletal reefs (*sensu* Riding, 2002; see also figs 12 and 16 in Racki, 1993; fig. 10 in Wolniewicz, 2021; fig. 27 in Halamski *et al.*, 2022), and the extent of downslope redeposition of the skeletal material to the outer ramp (arrow), ranging into the lagoonal domain (broken line). The homoclinal slope profile is strongly exaggerated.

interval, typified by disordered fabrics (microfacies RMF 9 of Flügel, 2010; see also SMF 10 of Wilson, 1975), that is, chaotic accumulation of variably sized, frequently broken, and/or abraded coral and stromatoporoid skeletons and several cm-size micritic intraclasts in a bioclast-rich micrite matrix (Figs 4D, 6). These characteristics imply large-scale destructive processes during high-energy deposition, which resulted in the massive down-slope transfer of unsorted sediments with major clasts from eroded reef shoals. The processes contrast with waning storm/current action, recorded in many (most?) limestone layers as distal tempestites, but with the primary fabrics destroyed by bioturbators.

In summary, sediments of the Skały Fm in the Miłoszów sections were formed in open-marine environments in the lower part of the Łysogóry ramp slope in relatively quiet-water environments. However, they were close to the storm-wave base, as evidenced by the episodic and negligible influence of higher-energy events, such as storms, or occasional bottom currents. As stressed by Flügel (2010, p. 718), the low-energy, mud-dominated ramps were mainly controlled by waves and tides. The scoured organic buildups were, thus, a prolific and persistent source of fine debris and calcareous ooze, transported together with rarer reef builder/dweller skeletons into peri-biohermal environments (as evidenced by the talus-like set M1-1a). Consequently, intraclastic coral biorudites of the tripartite M1-1b unit can be interpreted even as tsunami deposits, undervalued in epeiric domains (see Łuczyński *et al.*, 2014; Pratt and Rule, 2021), and reported from the coeval nearby Kielce carbonate bank in the large-scale fragmentation and onshore resedimentation of stromatoporoid skeletons (Łuczyński, 2022). On the other hand, significant downslope transport and redeposition is confirmed also by the ecologically mixed assemblage of skeletal grains. Stenohaline open-marine reef-dwelling corals, massive stromatoporoids, crinoids, and brachiopods, as well stenohaline echinoids and trilobites co-occur commonly with calcispheres and rarer amphiporoids (Fig. 5F–H, P; Appendix 2), the latter two typical of restricted lagoons of inner ramp settings (facies 11D and 12D of Wilson, 1975; zone IIIb of Machel and Hunter, 1994; e.g., Kaźmierczak, 1976; Racki and Soboń-Podgórska, 1993; Zapalski *et al.*, 2022; Fig. 12). Such high-energy processes are evidenced particularly in the Givetian-Frasnian Szydłówek Beds developed in the Kostomłoty zone (Racki *et al.*, 2004; Jagt-Yazykova *et al.*, 2006). In particular, the calcareous microorganisms of unknown biological affinity (partly represented by volvocae green algae and calcified acritarchs; Kaźmierczak and Kremer, 2005; Fig. 5F–H) were easily washed to the deeper slope zones, either from localized pond areas within the wave-dominated ramp barrier belt (later eroded over the Łysogóry Anticline) or from the vast back-barrier lagoon of the *Stringocephalus* biostromal bank of the Kielce Region (Racki, 1993; Wolniewicz, 2021; Halamski *et al.*, 2022). The last case implies rather unusual, tsunami-type sedimentary reworking (Łuczyński, 2022).

The investigated succession was formed close to the photic zone because photoautotrophic organisms, such as green algae, girvanellids and *Steneiria*-like cyanobacteria

(e.g., Zhou and Pratt, 2019), occur throughout the entire succession. This could be partly in agreement with the conclusions of Dubicka *et al.* (2021) and Zapalski *et al.* (2022) who described, from Miłoszów limestones, photosynthetically active foraminifera and mesophotic tabulate corals. However, the topmost part of the Skały Fm in locality M0, distinguished by the incipient mesophotic biostrome (layer 9; Halamski *et al.*, 2022) and the appearance of *Steneiria*-like cyanobacteria, may have been deposited in a little deeper- and/or quieter-water conditions. This waning ooze and debris transfer from carbonate sources, evidenced in the declining CaCO<sub>3</sub> content, is traced also in the distinctly decreasing abundance of calcispheres and other foraminifera-like microfossils, and the total disappearance of semitextularid foraminifers (Fig. 12), green algae, and coral colonies (see Tab. 2). The clay-rich strata of Świętomarz Beds exhibit continuation of this trend, concluding with the impoverished skeletal content in the top sample M0-10D, dominated by diminutive ostracods (Fig. 7).

Ubiquitous bioerosion in eutrophic settings is reflected in common microborings, particularly in crinoid bioclasts (Figs 5D, 6B), and rarer micrite envelopes; a potential mud-producing role of calcispheres (Berkyová and Munnecke, 2010) is also noteworthy. Additionally, thriving large deposit-feeder and suspension-feeder populations, including the diverse encrusting communities reported by Zatoń and Wrzolek (2020), indicate high nutrient levels, both within the bottom muds and suspended in the water column. A tendency toward eutrophication seems to be a specific character of the outer ramp zone in the Łysogóry Region, at least in reference to Flügel's (2010) ramp model. This supposition is confirmed by the mostly bored crinoid columnals, reported by Głuchowski (2005) from the Eifelian part of the Skały Fm in the type section (see also Gorzelak *et al.*, 2011 for an inferred crinoid record of placoderm bite marks).

In the light of the geochemical proxies, the Skały Formation was deposited in a well-oxygenated marine environment, influenced by a continuous but varying intensity input of terrigenous material. The dominance of miospores originating on land in all study sections, the low content of amorphous organic matter, and rare scolecodonts and acritarchs (Fig. 11F; Kondas and Filipiak, 2022) further confirm these observations. The changing proportions of terrestrial and marine organic matter is reflected in the  $\delta^{13}\text{C}_{\text{org}}$  record. The negative anomaly  $\delta^{13}\text{C}_{\text{org}}$  in the M0 section correlates with marly intervals with a rich assemblage of open-marine organisms (samples M0-4A, B; Fig. 7) and the highest values for the intensive input of marine debris (see miospore and acritarch frequency in Fig. 11F).

## REGIONAL ASPECTS OF THE PRE-TAGHANIC ECOSYSTEM

The gentle slope profiles of carbonate ramps are viewed as efficient in subduing the most high-energy depositional events in middle shelf settings that resulted in an omnipresence of muddy deposits and the suppressed massive

framebuilding in reef shoals and isolated buildups (Wilson, 1975, p. 362; Flügel, 2010; see also reviews in: Read, 1985; Machel and Hunter, 1994; Reijmer, 2021). As shown in the present study, the soft-bottom habitats of the Łysogóry ramp, marked by well-aerated and illuminated and eutrophic conditions, were places of diverse benthos blooming, both in infaunal and epifaunal niches. In the Moroccan intrashelf setting, Kaufmann (1998) showed that it is difficult to subdivide the Early Givetian ramp facies of the high-latitude Mader Basin by means of distinctive hydrodynamic interfaces (see also Wendt *et al.*, 1997 and Jakubowicz *et al.*, 2019). Despite a location within the equatorial belt, this hindrance is also visible in the coeval fragmentary Miłoszów succession (see a more general summary in Halamski *et al.*, 2022). Only two generalized facies can be distinguished with certainty: (1) shallower (middle) ramp, affected by episodic high-energy conditions in the euphotic zone, and (2) deeper (outer) ramp, encompassing mostly mesophotic low-energy habitats (Fig. 12; compare the Czech ramp examples in Bábek *et al.*, 2018 and a Canadian summary in Machel and Hunter, 1994).

Following Halamski *et al.* (2022, fig. 27), with reference to the standard Struve's (1963) biofacies model of the Middle Devonian 'reefs' in the Eifel Mts, two main sessile epifauna groupings include (1) shelly nests and clusters formed by low-diversity brachiopod communities (dominated in the deepest part by small-sized *Bifida* and *Echinocoelia*; Fig. 7), and (2) ephemeral mesophotic coral biostromes, with a prominent example of tabulate marly biostrome (unit M1-IIa), 'a hot spot' of benthos diversity (note also the brachiopod- and coral-rich layer M0-9). In the light of the present data, the brachiopod milieu (Brachiopodetum), interfingering partly with coral-dominated Rapetum and Cespitetum zones (fig. 27 in Halamski *et al.*, 2022), was inhabited by at least two additional biota, which are as follows:

1. Bryozoan bioconstructions (with a contribution of octactinellid calcisponges?), encompassing low-relief biostromes and patches, formed mainly by sediment stabilizing branched colonies (A. Ernst, mail comm., 2022), including delicate cryptostomes (*Isostylus*?) and cystoporates (*Sulcoretepora*), and fenestrates (pinnate *Penniretepora*). The faunal association occurs abundantly in the marly levels of the M0 section (see Fig. 7), and diverse bryozoans, dominated by erect trepostomate species, are reported as well as by Wyse Jackson (in Halamski *et al.*, 2022) from the marly coral biostrome (unit M1-IIa);
2. Localized crinoid clumps. The mass-occurring fine crinoid debris (mostly less than 2 mm in size) may be interpreted as distal evidence of prolific crinoid meadows of the mid-slope zone (Crinoidetum; see Fig. 6B). However, a parautochthonous record of diminutive crinoid populations, colonizing shell pavements, is probable in the muddy habitats.

Two major events are recognized as the main perturbations in the overall steady calcareous-clayey depositional system:

- the Early Givetian time of intensive reworking of the ramp environments during three(?) extreme storm or

- tsunami episodes, followed by the rapid but transient cessation of carbonate deposition within the middle part of the Skały Fm (recorded in the M1-I/M1-II transition);
- the Middle Givetian demise of the Łysogóry carbonate ramp, evidenced in the stepwise diachronous passage from the Skały Fm to the Świętomarz Beds (Malec, 2012; Racki *et al.*, 2022); the carbonate factory only briefly revived in the Łysogóry Region during bioherm growth of the Pokrzywianka Beds (Zatoń *et al.*, 2022).

The older high-energy episode needs to be investigated in a broader, regional perspective, including lateral facies changes, while more data already may be available on the second depositional turnover, studied in the M0 succession. Dominantly carbonate deposition and short-lived benthos colonization were influenced by siliciclastic input (layers 4 and 8). Relatively low sea-level during the pre-Taghanic interval and probable climatic fluctuations (Fig. 11) could be manifested in intensified chemical weathering in sediment source domains. On the one hand, intensive supply of clayey material may have provided the nutrients necessary to stimulate primary productivity; on the other hand, it may have reduced water transparency and negatively affected photosynthetic activity on the seafloor, as indicated at the Skały section (Dubicka *et al.*, 2021).

The environmental changes at the top of the Skały Formation are reflected in the onset of clay-controlled sedimentation, which resulted from the suppressed input of calcareous material, as recorded in micropalaeontological trends (e.g., the disappearance of semitextularids; Fig. 7) and palynofacies changes (the increasing frequency of marine acritarchs, Fig. 11F). The carbonate production crisis is presumably a record of the collapse of the carbonate factory at the northern periphery of the Kielce platform (Narkiewicz *et al.*, 2006). The ramp succession graded upward into the prodelta facies of the Świętomarz Beds (Malec, 2012; Zatoń *et al.*, 2022; Fig. 7). The Middle Givetian event was considered the combined effect of tectonic activation and/or climatic changes in the area, situated to the south-east of the Holy Cross region (Czarnocki, 1957; Kłossowski, 1985; Malec, 2012), paired with the pre-IIa sea-level fall (Narkiewicz *et al.*, 2011). The petrographic data of Kuleta and Malec (2015) indeed indicate a hypothetically active orogenic-cratonic source area (i.e., a recycled orogen built of siliciclastic rocks and a cratonic continental zone) in western Volhynia (Ukraine), but it is impossible to assess the magnitude of the tectonic movements.

According to Turnau and Racki (1999, fig. 8) and Kondas and Filipiak (2022), the regional transition was promoted by a transgression, and the biotic and geochemical variations (Figs 7–9) are indicative of the influx of <sup>12</sup>C-rich, oligotrophic marine water. The dynamic interplay between a carbonate platform and an intermittently prograding delta front was clearly recorded in the silty-sandy intervals in the upper part of the Skały Fm (Pajchłowa, 1957; Malec and Turnau, 1997; Racki *et al.*, 2022a), and finally, in the marly layers of the M0 section (Fig. 7). The final onset of a prodelta muddy regime might have occurred without a significant sea-level change, when driven by a mass influx of fine clastics and turbid waters from tectonically restructured areas because of block movements. It is noteworthy

that the dispersal of pelagic biota (styliolinids, small-sized bivalves), known from the Skały Fm (Pajchlowa, 1957), especially in the Świętomarz-Śniadka section (Woroncowa-Marcinowska, 2012), is unrecognizable in the more proximal Miłoszów and Skały successions during the eventual carbonate crisis (see also Malec and Turnau, 1997). This lateral ecological segregation may be explained by low-salinity proximal watermasses in the estuarine-type circulation, promoted by the expanding delta (see the Givetian Hamilton-Tully biofacies example from Appalachian Basin in Zambito *et al.*, 2012; Fig. 13).

### A CONUNDRUM OF *PUMILIO* GLOBAL EVENT IN ŁYSOGÓRY BASIN

Among the Miłoszów localities, the Middle Givetian coquinooid accumulations, if any, may occur exclusively in the M0 section (in bed M3λ the rich shelly fauna is found in the form of localised nests; Baliński and Halamski, in press). The absence of a distinct positive  $\delta^{13}\text{C}$  excursion in carbonate and organic signatures (Fig. 10) and the dark grey limestone with increased brachiopod-styliolinid abundance indicates that the *pumilio* event is not recognized, either because of a missing section or because it did not affect this local area at all. In the investigated localities, single small brachiopods similar to the *Pumilio*-like fauna (cf. Lottmann, 1990b) are visible in thin sections; however, they probably represent the genus *Bifida*, which is not related to *pumilio* event.

Conversely, the upper *pumilio* level was hypothesized by Woroncowa-Marcinowska (2012, p. 359) as developed in the styliolinid-rich shaly succession with goniatites in the Świętomarz-Śniadka section. Thus, this attractive topic is still a challenge for further research in both areas of the Skały

Fm exposure, exemplified by the obvious biogeographic question: why were distant Moroccan (= Gondwanan) localities more similar to the Rhenish sites than these in the Holy Cross Mts, also located in the southern Laurussian shelf? This puzzle is unveiled once again by the Late Givetian rhynchonellide brachiopod succession in the Kostomłoty basin (Sartenaer and Racki, 1992).

### CONCLUSIONS

1. Three Lower to Middle Givetian marly-limestone successions, exposed at Miłoszów, represent middle to outer facies belts of the vast carbonate ramp, characterized by largely rich epifaunal and infaunal benthic life in muddy, mostly oxic, eutrophic, and sunlit habitats. Brachiopods and periodically corals (in mesophotic association), erect branching bryozoans, and most likely tiny crinoids played a leading role among flourishing, sessile suspension-feeders.
2. Subdued storm events and intensified current circulation, possibly enhanced by a tsunami (tsunamis?) in a brief early Givetian time interval, controlled prolific carbonate ooze shedding from shallow ramp areas, including restricted back-ramp lagoons and a variety of organic buildups populated by corals and stromatoporoids. The ecologically mixed grain association is indicated by a rich occurrence of calcispheres and amphiporoids, being a typical lagoonal biota in the deep ramp facies.
3. The effective carbonate factory declined stepwise regionally during the Middle Givetian because of an intermittent westward progradation of the deltaic system of the Świętomarz Beds, influenced probably by activation of block movements in western Volhynia. The regional carbonate crisis resulted in the regional demise of diverse benthic life, including prolific calcified microbiota.

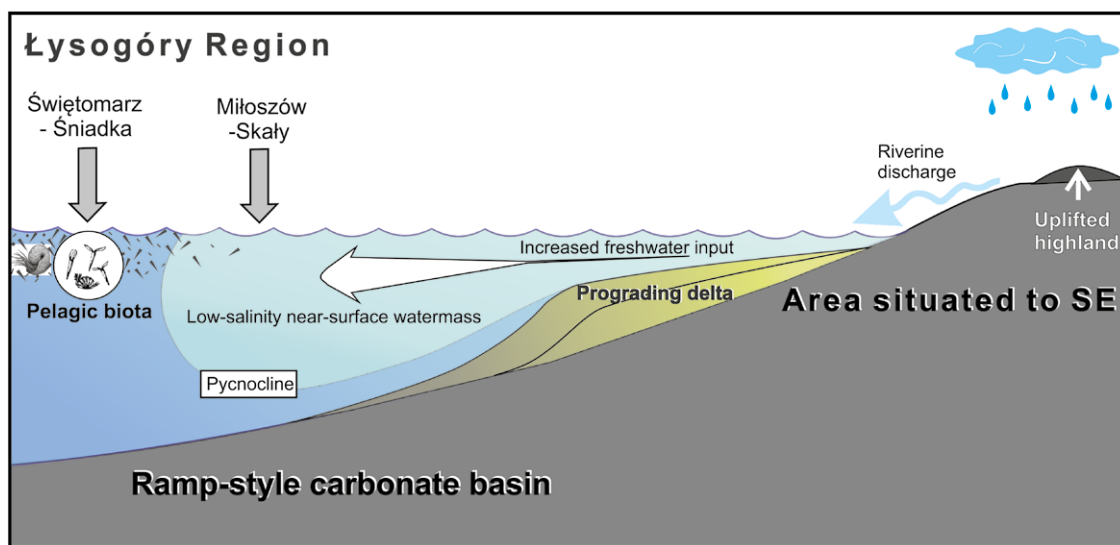


**Fig. 13.** An idealized model of quasi-estuarine - type circulation, developed in the initial progradation phase of the Givetian delta into the Łysogóry Region (i.e., the transition from the Skały Fm to the Świętomarz Beds; after data from Malec, 2012; Kuleta and Malec, 2015). This oceanographic pattern resulted from increased river flow and, consequently, enhanced freshwater input from the uplifted southeast hinterland to the carbonate ramp (based on the model for the Middle Givetian Appalachian Basin in Zambito *et al.*, 2012, fig. 10B; see also fig. 1C in Edinger *et al.*, 2002). The subsurface brackish watermass is interpreted as a stressor, responsible for the exclusion of pelagic biota in the proximal region of Skały-Miłoszów.

4. The higher Skały Fm succession, deposited between the important Kačák and Taghanic biotic crises, is noticeable for a background carbon-isotope pattern in carbonate and organic matter signatures, with the baseline  $\delta^{13}\text{C}_{\text{carb}}$  values between 1‰ and 2‰. The  $\delta^{13}\text{C}$  patterns, observed in the Miłoszów sections, confirm therefore a stabilized carbon cycle and common environmental stasis in the global ecosystem in the studied Givetian interval (see discussion in Halamski *et al.*, 2022). However, the strata studied represent a small fraction of the Skały Fm, and more refined biogeochemical and ecological records are a challenge for future work.
5. The microfacies and carbon isotope data confirm that at least the lower *pumilio* event was not recorded in the Łysogóry Region. This problem is another attractive topic to explore, especially in the unresolved, biogeographic perspective, between the Laurussian and Gondwanan epeiric seas.

### Acknowledgements

We thank Waldemar Bardziński, Mariusz Gardocki and Tomasz Wrzolek (Institute of Earth Sciences, University of Silesia in Katowice) for laboratory work, Adam T. Halamski (Institute of Paleobiology, Polish Academy of Sciences) for his assistance with the fieldwork and editorial handling. We appreciated the thoughtful suggestions and critical remarks from Brian R. Pratt (Department of Geological Sciences, University of Saskatchewan) and James J. Zambito (Department of Geology, Beloit College). The research was supported by NCN Grants 2018/29/B/ST10/01811 “Systematic affiliation and palaeoenvironmental significance of Mid-Paleozoic calcareous microfossils (protists and microproblematica)” and 2016/23/B/ST10/02744 “Evolution and palaeobiogeography of Devonian brachiopod faunas on the South Polish shelf before and after the global Taghanic event” (for Andrzej Baliński, Institute of Paleobiology, Polish Academy of Sciences). Barbara Kremer (Institute of Paleobiology, Polish Academy of Sciences) is thanked for providing data and the photographs for Figure 7 and Tomasz Wrzolek for the photograph in Figure 6. Andrej Ernst (University of Hamburg) kindly identified the bryozoan specimens, while Carlton Brett (University of Cincinnati) greatly improved the eustatic and climatic data in Figure 11D–E.

### REFERENCES

- Aboussalam, Z. S. & Becker, R. T., 2011. The global Taghanic Biotic Crisis (Givetian) in the eastern Anti-Atlas, Morocco. *Palaeogeography, Palaeoclimatology, Palaeoecology*, 304: 136–164.
- Algeo, T. J. & Lyons, T. W., 2006. Mo-total organic carbon covariation in modern anoxic marine environments: Implications for analysis of paleoredox and paleohydrographic conditions. *Paleoceanography*, 21: 1–23.
- Algeo, T. J. & Maynard, J. B., 2008. Trace-metal covariation as a guide to water-mass conditions in ancient anoxic marine environments. *Geosphere*, 4: 872–887.
- Allan, J. R. & Matthews, R. K., 1982. Isotope signatures associated with early meteoric diagenesis. *Sedimentology*, 29: 797–817.
- Bábek, O., Faměra, M., Šimíček, D., Weinerová, H., Hladil, J. & Kalvoda, J., 2018. Sea-level changes vs. organic productivity as controls on Early and Middle Devonian bioevents: Facies- and gamma-ray based sequence-stratigraphic correlation of the Prague Basin, Czech Republic. *Global and Planetary Change*, 160: 75–95.
- Baird, G. C. & Brett, C. E., 2008. Late Givetian Taghanic bioevents in New York State: new discoveries and questions. *Bulletin of Geosciences*, 83: 357–370.
- Baliński, A. & Halamski, A. T., (in press). Pre-Taghanic (Lower to lower Middle Givetian) brachiopods from Miłoszów in the Holy Cross Mountains (Poland). *Annales Societatis Geologorum Poloniae*, 93.
- Barham, M., Joachimski, M. M., Murray, J. & Williams, D. M., 2012. Diagenetic alteration of the structure and  $\delta^{18}\text{O}$  signature of Palaeozoic fish and conodont apatite: potential use for corrected isotope signatures in palaeoenvironmental interpretation. *Chemical Geology*, 298–299: 11–19.
- Becker, R. T., Gradstein, F.-M. & Hammer, O., 2012. The Devonian Period. In: Gradstein, F. M., Ogg, J. G., Schmitz, M. & Ogg, G. (eds), *The Geologic Time Scale 2012*. Elsevier, Amsterdam, Boston, pp. 559–601.
- Becker, R. T., Königshof, P. & Brett, C. E., 2016. Devonian climate, sea level and evolutionary events: an introduction. In: Becker, R. T., Königshof, P. & Brett, C. E. (eds), *Devonian Climate, Sea Level and Evolutionary Events*. Geological Society, London, Special Publications, 423: 1–10.
- Becker, R. T., Marshall, J. E. A. & Da Silva, A.-C., 2020. The Devonian period. With contributions by F. P. Agterberg, F. M. Gradstein and J. G. Ogg. In: Gradstein, F. M., Ogg, J. G., Schmitz, M. D. & Ogg, G. M. (eds), *Geologic Time Scale, Volume 2*. Elsevier, pp. 733–810.
- Berkyová, S. & Munneke, A., 2010. “Calcspheres” as a source of lime mud and peloids – evidence from the early Middle Devonian of the Prague Basin, the Czech Republic. *Bulletin of Geosciences*, 85: 585–602.
- Blood, D. R., Lash, G. G. & Bridges, L. C., 2013. Biogenic silica in the Devonian shale succession of the Appalachian Basin, USA. *Search and Discovery Article 50864*. AAPG/Datapages, Inc. [http://www.searchanddiscovery.com/documents/2013/50864blood/ndx\\_blood.pdf](http://www.searchanddiscovery.com/documents/2013/50864blood/ndx_blood.pdf) [27.10.2022.]
- Brand, U., Jiang, G., Azmy, K., Bishop, J. & Montañez, I. P., 2012. Diagenetic evaluation of a Pennsylvanian carbonate succession (Bird Spring Formation, Arrow Canyon, Nevada, U.S.A.) – 1: Brachiopod and whole rock comparison. *Chemical Geology*, 308: 26–39.
- Brett, C. E., Baird, G. C., Bartholomew, A., DeSantis, M. & Ver Straeten, C., 2011. Sequence stratigraphy and revised sea level curve for the Middle Devonian of Eastern North America. *Palaeogeography, Palaeoclimatology, Palaeoecology*, 304: 21–53.
- Brett, C. E., Zambito, J. J., IV, McLaughlin, P. I. & Emsbo, P., 2020. Revised perspectives on Devonian biozonation and environmental volatility in the wake of recent time-scale revisions. *Palaeogeography, Palaeoclimatology, Palaeoecology*, 549: 108843.
- Buggisch, W. & Joachimski, M. M., 2006. Carbon isotope stratigraphy of the Devonian of Central and Southern Europe. *Palaeogeography, Palaeoclimatology, Palaeoecology*, 240: 68–88.

- Calvert, S. E. & Pedersen, T. F., 2007. Elemental proxies for palaeoclimatic and palaeoceanographic variability in marine sediments: interpretation and application. *Developments in Marine Geology*, 1: 567–644.
- Craigie, N., 2018. *Principles of Elemental Chemostratigraphy. A Practical User Guide*. Springer, Cham, 189 pp.
- Czarnocki, J., 1957. Prace geologiczne. T. II, Geologia regionu lysogórskiego. Stratygrafia i tektonika Gór Świętokrzyskich, z. 1. *Prace Państwowego Instytutu Geologicznego*, 18: 1–138. [In Polish.]
- Dubicka, Z., Gajewska, M., Kozłowski, W., Hallock, P. & Hohenegger, J., 2021. Photosynthetic activity in Devonian Foraminifera. *Biogeosciences*, 18: 5719–5728.
- Edinger, E. N., Copper, P., Risk, M. J. & Atmojo, W., 2002. Oceanography and reefs of recent and Paleozoic tropical epicontinental seas. *Facies*, 47: 127–149.
- Flügel, E., 2010. *Microfacies of Carbonate Rocks – Analysis, Interpretation and Application*. Springer, Heidelberg, 984 pp.
- Fraser, T. A. & Hutchison, M. P., 2017. Litho-geochemical characterization of the Middle–Upper Devonian Road River Group and Canol and Imperial formations on Trail River, east Richardson Mountains, Yukon: age constraints and a depositional model for fine-grained strata in the Lower Paleozoic Richardson trough. *Canadian Journal of Earth Sciences*, 54: 731–765.
- Gajewska, M., 2022. Middle Devonian Foraminifera from the Holy Cross Mountains (Poland). *Annales Societatis Geologorum Poloniae*, 92: 411–424. [This issue.]
- García-Alcalde, J. L., 2010. Givetian brachiopod faunas of the Palentian Domain (N Spain). *Revista Española de Paleontología*, 25: 43–69.
- Głuchowski, E., 2005. Epibionts on Upper Eifelian crinoid columns from the Holy Cross Mountains, Poland. *Acta Palaeontologica Polonica*, 50: 315–328.
- Gorzela, P., Rakowicz, Ł., Salamon, M. A. & Szrek, P., 2011. Inferred placoderm bite marks on Devonian crinoids from Poland. *Neues Jahrbuch für Paläontologie und Geologie, Abhandlungen*, 259: 105–112.
- Grossman, E. L. & Joachimski, M. M., 2022. Ocean temperatures through the Phanerozoic reassessed. *Scientific Reports*, 12: 8938.
- Halamski, A. T., 2022. Middle Devonian biota and environments of the Lysogóry Region (Poland) – Introduction. *Annales Societatis Geologorum Poloniae*, 92: 317–321. [This issue.]
- Halamski, A., Baliński, A., Racki, G., Amler, M. R. W., Basse, M., Denayer, J., Dubicka, Z., Filipiak, P., Kondas, M., Krawczyński, W., Mieszkowski, R., Narkiewicz, K., Olempska, E., Wrzolek, T., Wyse Jackson, P. N., Zapalski, M. K., Zatoń, M. & Kozłowski, W., 2022. The pre-Taghanic (Givetian, Middle Devonian) ecosystems of Miłoszów (Holy Cross Mts, Poland). *Annales Societatis Geologorum Poloniae*, 92: 323–379. [This issue.]
- Hall, D., Sterner, M. & Shukla, R., 2013. Application of cuttings gas/oil analysis, rapid XRF and high-resolution photography to reservoir evaluation. *World Oil*, April 2013 issue, pp. 163–168.
- Hildred, G. V. & Rice, C., 2014. Using high resolution chemostratigraphy to determine well-bore pathways in multilateral drilling campaigns: an example from the Horn River Formation, British Columbia, Canada. *Extended abstract presented at SCPG/CSEG/CWLS GeoConvention 2012*. TELUS Convention Centre and ERBC Core Research Centre, Calgary. [www.searchanddiscovery.com/documents/2014/80362hildred/ndx\\_hildred](http://www.searchanddiscovery.com/documents/2014/80362hildred/ndx_hildred) [27.10.2022.]
- House, M. R., 2002. Strength, timing, setting and cause of mid-Palaeozoic extinctions. *Palaeogeography, Palaeoclimatology, Palaeoecology*, 181: 5–25.
- Jagt-Yazykova, E. V., Krawczyński, W. & Rakociński, M., 2006. Molluscs from the Early Frasnian Goniatic Level at Kostomłoty in the Holy Cross Mountains, Poland. *Acta Palaeontologica Polonica*, 51: 707–718.
- Jakubowicz, M., Król, J., Zapalski, M. K., Wrzolek, T., Wolniewicz, P. & Berkowski, B., 2019. At the southern limits of the Devonian reef zone: palaeoecology of the Aferdou el Mrakib reef (Givetian, eastern Anti-Atlas, Morocco). *Geological Journal*, 54: 10–38.
- Joachimski, M. M., 1994. Subaerial exposure and deposition of shallowing upward sequences: evidence from stable isotopes of Purbeckian peritidal carbonates (basal Cretaceous), Swiss and French Jura Mountains. *Sedimentology*, 41: 805–824.
- Joachimski, M. M., Breisig, S., Buggisch, W., Talent, J. A., Mawson, R., Gereke, M., Morrow, J. R., Day, J. & Weddige, K., 2009. Devonian climate and reef evolution: Insights from oxygen isotopes in apatite. *Earth and Planetary Science Letters*, 284: 599–609.
- Johnson, J. G., Klapper, G. & Sandberg, C. A., 1985. Devonian eustatic fluctuations in Euramerica. *Geological Society of America Bulletin*, 96: 567–587.
- Kabanov, P., Gouwy, S., van der Boon, A. & Grasby, S. E., 2022. Nature of Devonian anoxic events based on multiproxy records from Panthalassa, NW Canada. *SSRN Electronic Journal*, <https://doi.org/10.2139/ssrn.4140260> [27.10.2022].
- Kaufmann, B., 1998. Middle Devonian reef and mud mounds on a carbonate ramp: Mader Basin (eastern Anti-Atlas, Morocco). In: Wright, V. P. & Burchette, T. P. (eds), *Carbonate Ramps. Geological Society Special Publications*, 149: 417–435.
- Kaźmierczak, J., 1976. Volvocacean nature of some Palaeozoic non-radiosphaerid calcispheres and parathuraminid ‘foraminifera’. *Acta Palaeontologica Polonica*, 21: 245–258.
- Kaźmierczak, J. & Kremer, B., 2005. Post-mortem calcified Devonian acritarchs as a source of calcispheric structures. *Facies*, 51: 554–565.
- Kiipli, E., Kiipli, T., Kallaste, T. & Siir, S., 2012. Al<sub>2</sub>O<sub>3</sub>/TiO<sub>2</sub> ratio of the clay fraction of Late Ordovician–Silurian carbonate rocks as an indicator of paleoclimate of the Fennoscandian Shield. *Palaeogeography, Palaeoclimatology, Palaeoecology*, 365–366: 312–320.
- Kłossowski, J., 1985. Middle Devonian sedimentation in the Lysogóry region (Świętomarz–Śniadka section). *Przegląd Geologiczny*, 33: 264–267. [In Polish, with English summary.]
- Kondas, M. & Filipiak, P., 2022. Middle Devonian (Givetian) palynology of the northern Holy Cross-Mountains (Miłoszów, south-central Poland). *Review of Palaeobotany and Palynology*, 301: 104629.
- Konon, A., 2007. Buckle folding in the Kielce Unit, Holy Cross Mountains, central Poland. *Acta Geologica Polonica*, 57: 415–441.

- Königshof, P., Nesbor, H.-D. & Flick, H., 2010. Volcanism and reef development in the Devonian: a case study from the Lahn syncline, Rheinisches Schiefergebirge (Germany). *Gondwana Research*, 17: 264–280.
- Kuleta, M. & Malec, J., 2015. Petrographic study of the Middle Devonian Świętomarz Beds of the Holy Cross Mountains and the Żniatyń Member from the SE Lublin area. *Biuletyn Państwowego Instytutu Geologicznego*, 463: 43–62. [In Polish, with English summary.]
- Lim, D., Kim, H., Kim, J., Jeong, D. & Kim, D., 2020. Mercury proxy for hydrothermal and submarine volcanic activities in the sediment cores of Central Indian Ridge. *Marine Pollution Bulletin*, 159: 111513.
- Lottmann, J., 1990a. Die *pumilio*-Events (Mittel-Devon). *Göttinger Arbeiten zur Geologie und Paläontologie*, 44: 1–98.
- Lottmann, J., 1990b. The Middle Givetian *pumilio*-Events a tool for high time resolution and event-stratigraphical correlation. In: Kauffman, E. G. & Walliser, O. H. (eds), *Extinction Events in Earth History. Lecture Notes in Earth Sciences, Volume 30*. Springer, Berlin, Heidelberg, pp. 145–149.
- Luczyński, P., 2022. Tsunamites versus tempestites: Various types of redeposited stromatoporoid beds in the Devonian of the Holy Cross Mountains (Poland), a case study from the Ołowianka Quarry. *PLoS ONE*, 17: e0268349.
- Luczyński, P., Skompski, S. & Kozłowski, W., 2014. Stromatoporoid beds and flat-pebble conglomerates interpreted as tsunami deposits in the upper Silurian of Podolia, Ukraine. *Acta Geologica Polonica*, 64: 261–280.
- Machel, H. G. & Hunter, I. G., 1994. Facies models for Middle to Late Devonian shallow-marine carbonates, with comparisons to modern reefs: a guide for facies analysis. *Facies*, 30: 155–176.
- Malec, J., 2012. The Middle Devonian Świętomarz beds of the Holy Cross Mts. in the light of sedimentological study. *Biuletyn Państwowego Instytutu Geologicznego* 452: 131–166. [In Polish, with English summary.]
- Malec, J. & Turnau, E., 1997. Middle Devonian conodont, ostracod and miospore stratigraphy of the Grzegorzowice–Skały section, Holy Cross Mountains, Poland. *Bulletin of the Polish Academy of Sciences, Earth Sciences*, 45: 67–86.
- McGhee, G. R., Clapham, M. E., Sheehan, P. M., Bottjer, D. J. & Droser, M. L., 2013. A new ecological-severity ranking of major Phanerozoic biodiversity crisis. *Palaeogeography, Palaeoclimatology, Palaeoecology*, 370: 260–270.
- Narkiewicz, K. & Königshof, P., 2018. New Middle Devonian conodont data from the Dong Van area, NE Vietnam (South China Terrane). *Paläontologische Zeitschrift*, 92: 633–650.
- Narkiewicz, M., Narkiewicz, K. & Turnau, E., 2011. Devonian depositional development of the Łysogóry-Radom and Lublin Basins (south-eastern Poland). In: Narkiewicz, M. (ed.) *Devonian basins of south-eastern Poland. Prace Państwowego Instytutu Geologicznego*, 196: 289–318.
- Narkiewicz, M., Racki, G., Skompski, S. & Szulczewski, M., 2006. Procesy i zdarzenia w historii geologicznej Gór Świętokrzyskich. In: Skompski, S. & Żylińska, A. (eds), *Materiały konferencyjne, LXXVII Zjazd Naukowy Polskiego Towarzystwa Geologicznego, Ameliówka k. Kielc 28–30 czerwca 2006 r.*, pp. 51–77. [In Polish.]
- Pajchłowa, M., 1957. The Devonian in the Grzegorzowice-Skały section. *Biuletyn Instytutu Geologicznego*, 122: 145–254. [In Polish, with English summary.]
- Pettijohn, F. J., 1957. *Sedimentary Rocks, 2nd Edition*. Harper, New York, pp. 718.
- Pratt, P. R. & Rule, R. G., 2021. A Mesoproterozoic carbonate platform (lower Belt Supergroup of western North America): sediments, facies, tides, tsunamis and earthquakes in a tectonically active intracratonic basin. *Earth-Science Reviews*, 217: 103626.
- Pyle, L. J. & Gal, L. P., 2016. Reference section for the Horn River Group and definition of the Bell Creek Member, Hare Indian Formation in central Northwest Territories. *Bulletin of Canadian Petroleum Geology*, 64: 67–98.
- Racki, G., 1993. Evolution of the bank to reef complex in the Devonian of the Holy Cross Mountains. *Acta Palaeontologica Polonica*, 37: 87–182.
- Racki, G., Mazur, S., Narkiewicz, K., Piszczowska, A., Bardziński, W., Kołtonik, K., Szymanowski, D., Filipiak, P. & Kremer, B., 2022b. A waning Saxothuringian Ocean evidenced in the Famennian tephra-bearing siliceous succession of the Bardo Unit (Central Sudetes, SW Poland). *Geological Society of America Bulletin*, 134: 2373–2398.
- Racki, G., Piechota, A., Bond, D. & Wignall, P. B., 2004. Geochemical and ecological aspects of lower Frasnian pyrite-ammonoid level at Kostomłoty (Holy Cross Mountains, Poland). *Geological Quarterly*, 48: 267–282.
- Racki, G. & Soboń-Podgórska, J., 1993. Givetian and Frasnian calcareous microbiotas of the Holy Cross Mountains. *Acta Palaeontologica Polonica*, 37: 255–289.
- Racki, G., Wójcik, K., Halamski, A. T. & Narkiewicz, M., 2022a. Middle Devonian Skały Formation in the Holy Cross Mountains (Poland) - formal description and subdivision based on a new field data. *Annales Societatis Geologorum Poloniae*, 92: 425–444. [This issue.]
- Rakociński, M., Marynowski, L., Zatoń, M. & Filipiak, P., 2021. The mid-Tournaisian (Early Carboniferous) anoxic event in the Laurussian shelf basin (Poland): an integrative approach. *Palaeogeography, Palaeoclimatology, Palaeoecology*, 566: 110236.
- Ratcliffe, R., Wright, M. & Spain, D., 2012. Unconventional methods for unconventional plays: using elemental data to understand shale resource plays – part 2. *Petroleum Exploration Society of Australia News*, 116: 55–60.
- Read, J. F., 1985. Carbonate platform facies models. *American Association of Petroleum Geologists Bulletin*, 69: 1–21.
- Reijmer, J. G., 2021. Marine carbonate factories: review and update. *Sedimentology*, 68: 1729–1796.
- Rubinowski, Z., 1969. Geologia, mineralizacja i geneza złóż siarczków żelaza typu Rudek w Górach Świętokrzyskich i metodyka ich poszukiwań. *Rocznik Polskiego Towarzystwa Geologicznego*, 39: 721–722. [In Polish.]
- Sageman, B. B. & Lyons, T. W., 2003. Geochemistry of fine-grained sediments and sedimentary rocks. In: Mackenzie, F. T. (ed.), *Treatise on Geochemistry*, 7: 115–158.
- Sartenaer, P. & Racki, G., 1992. A new late Givetian rhynchonellid species from the Holy Cross Mountains, Poland, and its relevance to stratigraphical and ecological problems near the Givetian/Frasnian boundary. *Bulletin de l'Institut royal des Sciences naturelles de Belgique, Sciences de la Terre*, 62: 61–73.
- Scotese, C. R., Song, H., Mills, B. J. W. & van der Meer, D. G., 2021. Phanerozoic paleotemperatures: the Earth's changing climate

- during the last 540 million years. *Earth-Science Reviews*, 215: 103503.
- Simon, L., Godderis, Y., Buggisch, W., Strauss, H. & Joachimski, M. M., 2007. Modeling the carbon and sulfur isotope compositions of marine sediments: climate evolution during the Devonian. *Chemical Geology*, 246: 19–38.
- Song, H., Wignall, P. B., Song, H., Dai, X. & Chu, D., 2019. Seawater temperature and dissolved oxygen over the past 500 million years. *Journal of Earth Sciences*, 30: 236–243.
- Stewart, E. M. & Ague, J. J., 2018. Infiltration-driven metamorphism, New England, USA: regional CO<sub>2</sub> fluxes and implications for Devonian climate and extinctions. *Earth and Planetary Science Letters*, 489: 123–134.
- Stricanne, L., Munnecke, A. & Pross, J., 2006. Assessing mechanisms of environmental change: palynological signals across the late Ludlow (Silurian) positive isotope excursion ( $\delta^{13}\text{C}$ ,  $\delta^{18}\text{O}$ ) on Gotland, Sweden. *Palaeogeography, Palaeoclimatology, Palaeoecology*, 230: 1–31.
- Struve, W., 1963. Das Korallenmeer der Eifel vor 300 Millionen Jahre-Funde, Deutungen, Probleme. *Natur Museum*, 93: 237–276.
- Struve, W., 1992. Neues zur Stratigraphie und Fauna des rhenotypen Mittel-Devon. *Senckenbergiana Lethaea*, 71: 503–624.
- Taylor, S. R. & McLennan, S., 1985. *The Continental Crust: its Composition and Evolution*. Blackwell Scientific Publications, Oxford, 312 pp.
- Tribouillard, N., Algeo, T. J., Baudin, F. & Riboulleau, A., 2012. Analysis of marine environmental conditions based on molybdenum-uranium covariation – applications to Mesozoic paleoceanography. *Chemical Geology*, 324–325: 46–58.
- Tribouillard, N., Algeo, T. J., Lyons, T. & Riboulleau, A., 2006. Trace metals as paleoredox and paleoproductivity proxies: an update. *Chemical Geology*, 232: 12–32.
- Turnau, E., 1996. Miospore stratigraphy of Middle Devonian deposits from Western Pomerania. *Review of Palaeobotany and Palynology*, 93: 107–125.
- Turnau, E., 2007. Palinostratygrafia. In: Matyja, H. (ed.), *Profile Głębokich Otworów Wiertniczych – Polskie Łąki PIG 1, 122*. Państwowy Instytut Geologiczny – Państwowy Instytut Badawczy, Warszawa, pp. 62–69. [In Polish.]
- Turnau, E., 2008. Wyniki badań palinostratygraficznych. In: Matyja, H. (ed.), *Profile Głębokich Otworów Wiertniczych – Jamno IG 1, IG2, IG3, 124*. Państwowy Instytut Geologiczny – Państwowy Instytut Badawczy, Warszawa, pp. 125–135. [In Polish.]
- Turnau, E. & Racki, G., 1999. Givetian palynostratigraphy and palynofacies: new data from the Bodzentyn Syncline (Holy Cross Mountains, central Poland). *Review of Palaeobotany and Palynology*, 106: 237–271.
- van Geldern, R., Joachimski, M. M., Day, J., Jansen, U., Alvarez, F., Yolkin, E. A. & Ma, X.-P., 2006. Carbon, oxygen and strontium isotope records of Devonian brachiopod shell calcite. *Palaeogeography, Palaeoclimatology, Palaeoecology*, 240: 47–67.
- van Hengstum, P. J. & Gröcke, D. R., 2008. Stable isotope record of the Eifelian–Givetian boundary Kačák-otomari Event (Middle Devonian) from Hungry Hollow, Ontario, Canada. *Canadian Journal of Earth Science*, 45: 353–366.
- Veizer, J., Ala, D., Azmy, K., Bruckschen, P., Buhl, D., Bruhn, F., Carden, G. A. F., Diener, A., Ebner, S., Goddérís, Y., Jasper, T., Korte, C., Pawellek, F., Podlaha, O. G. & Strauss, H., 1999.  $^{87}\text{Sr}/^{86}\text{Sr}$ ,  $\delta^{13}\text{C}$  and  $\delta^{18}\text{O}$  evolution of Phanerozoic seawater. *Chemical Geology*, 161: 59–88.
- Ver Straeten, C. A., Brett, C. E. & Sageman, B. B., 2011. Mudrock sequence stratigraphy: a multi-proxy (sedimentological, paleobiological and geochemical) approach, Devonian Appalachian Basin. *Palaeogeography, Palaeoclimatology, Palaeoecology*, 304: 54–73.
- Wedepohl, K. H., 1970. Geochemische Daten von sedimentären Karbonaten und Karbonatgesteinen in ihrem faziellen und petrogenetischen Aussagewert. *Verhandlungen der Geologischen Bundesanstalt*, 4: 692–705.
- Wedepohl, K. H., 1971. Environmental influences on the chemical composition of shales and clays. In: Ahrens, L. H., Press, F., Runcorn, S. K. & Urey, H. C. (eds), *Physics and Chemistry of the Earth*. Pergamon Press, Oxford, pp. 307–331.
- Wedepohl, K. H., 1991. The composition of the upper earth's crust and the natural cycles of selected metals. Metals in natural raw materials. Natural resources. In: Merian, E. (ed.), *Metals and Their Compounds in the Environment*. Verlag Chemie (VCH), Weinheim, pp. 3–17.
- Wendt, J., Belka, Z., Kaufmann, B., Kostrewa, R. & Hayer, J., 1997. The world's most spectacular carbonate mud mounds (Middle Devonian, Algerian Sahara). *Journal of Sedimentary Research*, 67: 424–436.
- Wilson, J. L., 1975. *Carbonate Facies in the Geologic History*. Springer, Berlin, 410 pp.
- Wolniewicz, P., 2021. From lagoons to mud mounds: palaeoecology of the Givetian to Frasnian stromatoporoids from the Holy Cross Mountains, Poland. *Lethaia*, 54: 378–398.
- Woroncowa-Marcinowska, T., 2012. Middle Devonian conodonts and structural implications for Świętomarz-Śniadka section (Holy Cross Mountains). *Annales Societatis Geologorum Poloniae*, 82: 349–360.
- Wright, A. M., Ratcliffe, K. T., Zaitlin, B. A. & Wray, D. S., 2010. The application of chemostratigraphic techniques to distinguish compound incised valleys in low-accommodation incised-valley systems in a foreland-basin setting: an example from the Lower Cretaceous Mannville Group and Basal Colorado Sandstone (Colorado Group), Western Canadian Sedimentary Basin. In: Ratcliffe, K. T. & Zaitlin, B. A. (eds), *Application of Modern Stratigraphic Techniques: Theory and Case Histories*. SEPM Special Publication, 94: 93–107.
- Yan, Y., Xia, B., Lin, G., Cui, X., Hu, X., Yan, P. & Zhang, F., 2007. Geochemistry of the sedimentary rocks from the Nanxiong Basin, South China and implications for provenance, paleoenvironment and paleoclimate at the K/T boundary. *Sedimentary Geology*, 197: 127–140.
- Yans, J., Corfield, R. M., Racki, G. & Prétat, A., 2007. Evidence for a major perturbation of the carbon cycle in the Middle Frasnian punctata conodont Zone. *Geological Magazine*, 144: 263–270.
- Zambito, J. J., Brett, C. E. & Baird, G. C., 2012. The Late Middle Devonian (Givetian) global Taghanic Biocrisis in its type area (Northern Appalachian Basin): geologically rapid faunal transitions driven by global and local environmental changes. In: Talent, J. A. (ed.), *Earth and Life. Global Biodiversity, Extinction Intervals and Biogeographic Perturbations Through Time*. Springer, Berlin, pp. 677–703.

- Zapalski, M. K., Król, J. J., Halamski, A. T., Wrzolek, T., Rakociński, M. & Baird, A. H., 2022. Coralliths of tabulate corals from the Devonian of the Holy Cross Mountains (Poland). *Palaeogeography, Palaeoclimatology, Palaeoecology*, 585: 1–11.
- Zatoń, M., Malec, J., Wrzolek, T., Kubiszyn, B. & Zapalski, M. K., 2022. Episkeletobionts of large rugose corals from the Middle Devonian mesophotic palaeoenvironment recorded in the Pokrzywianka Beds (Holy Cross Mountains, Poland). *Annales Societatis Geologorum Poloniae*, 92: 465–484. [This issue.]
- Zatoń, M. & Wrzolek, T., 2020. Colonization of rugose corals by diverse epibionts: dominance and syn vivo encrustation in a Middle Devonian (Givetian) soft-bottom habitat of the Holy Cross Mountains, Poland. *Palaeogeography, Palaeoclimatology, Palaeoecology*, 556: 109899.
- Zhou, K. & Pratt, B. R., 2019. Upper Devonian (Frasnian) stromatolite-bearing mud mounds, western Alberta, Canada: reef framework dominated by peloidal microcrystalline calcite. *Journal of Sedimentary Research*, 89: 833–848.



## Appendix 2

## Microfacies observations at the Miłoszów M1 and M0 sections.

Table A2.1

Detailed description of thin-sections from the Miłoszów M1 section.

Sample	Set	Description of microfacies
M1-6	Ib	Bioclastic packstone. Strongly fragmented skeletal grains are represented by crinoid ossicles, tabulate corals, bryozoans, brachiopods, molluscs, trilobites and smooth-shelled ostracods. Less frequent are echinoid spines, microconchids, rostroconchids and smooth-shelled ostracods.
M1-5	Ib	Coral floatstone/rudstone with peloids and isolated intraclasts in a micritic matrix. Fossils are represented by Rugosa corals and fragmented Rugosa and Tabulata corals, numerous crinoid ossicles, fragmented: brachiopods and molluscs, crinoids, massive stromatoporoids and smooth-shelled ostracods. Fossils in intraclasts are represented by fragmented crinoids, trilobites, brachiopods, molluscs and calcispheres. Fossils are strongly fragmented. Some of the bioclasts (especially crinoids) have microendolithic borings. Some corals are encrusted by stromatoporoids.
M1-4	Ia	Bioclastic-peloidal packstone. Numerous dolomite crystals. Fossils are represented by numerous crinoids, fragmented: brachiopods, ostracods, and tabulate corals and bryozoans. Other fossils consist of smooth-shelled ostracods, microconchids, amphiporoids, auloporids, girvanellids and other microbial bioclast overgrowths, calcispheres represented by <i>Parathuramina</i> , <i>Bisphaera</i> , <i>Radiosphaera</i> , <i>?Irregularina</i> . Additionally, green algae occur (probably genus <i>?Litaniaia</i> ), <i>Rotpletzella</i> and single small brachiopods. Fossils are strongly fragmented. Some of the bioclasts (especially crinoids) have microendolithic borings.
M1-3	Ia	Peloidal wackestone-packstone. Fossils are less numerous and consist of fragmented: tabulates, stromatoporoids, crinoids, trilobites, ostracods, molluscs and brachiopods. Numerous calcispheres occur (e.g., <i>Radiosphaera</i> , <i>Parathuramina</i> , Volvocales algae and <i>?Irregularina</i> ). Some of the bioclasts (stromatoporoids) have microendolithic borings.
M1-2B	Ia	Bioclastic packstone. Fossils are represented by abraded rugose corals, fragmented: tabulate corals, brachiopods, ostracods and trilobites. Other organisms are represented by smooth-shelled ostracods, crinoid ossicles, and single small brachiopods. Fossils are strongly fragmented. Some of the bioclasts have microendolithic borings.
M1/2A	Ia	Stromatoporoid floatstone. Other fossils are represented by Tabulata corals ( <i>?Heliolites</i> ), fragmented brachiopods, molluscs, crinoids and Rugosa corals, as well as smooth-shelled ostracods, gastropods and calcispheres. Stromatoporoids are overgrown by microbial shrubs (probably girvanellid). Fossils are strongly fragmented.
M1/1B	Ia	Bioclastic-peloidal packstone. Fossils are represented by fragmented: rugose and tabulate corals, crinoids, trilobites, ostracods, brachiopods and molluscs shells. Some bioclasts are overgrown by microbial girvanellid microstromatolites. Other fauna consist of calcispheres (e.g. <i>Parathuramina</i> , <i>Bisphaera</i> , <i>Radiosphaera</i> ), gastropods, amphiporoids, echinoid spines, foraminifers ( <i>Eonodosaria</i> ), <i>Rotpletzella</i> and algae ( <i>?Litaniaia</i> ).
M1/1A	Ia	Crinoid-brachiopod peloidal packstone. Fossils are represented by very numerous crinoid ossicles and fragments of brachiopods. Less numerous are smooth-shelled ostracods and their fragments, echinoid spines, gastropods, fragments of mollusc shells, foraminifers ( <i>?Tikhinella</i> ), fragmented tabulate corals, bryozoans, crinoids, trilobites, and calcispheres. Additionally, <i>Rotpletzella</i> occurs. Fossils are strongly fragmented. Some of the bioclasts (especially crinoids and molluscs) have microendolithic borings.

Table A2.2

Detailed description of thin-sections from the Miłoszów M0 section.

Sample	Description of microfacies
M0-9B	Wackestone/packstone with a micritic matrix. Fossils are represented by numerous crinoid ossicles and fragments of crinoids ossicles and fragments brachiopods, less numerous fragmented corals (Tabulata and Rugosa), trilobites, bryozoans, smooth-shelled ostracods and ferruginous ? <i>Stanieria</i> -like coccoidal cyanobacteria and sponge spicules. Fossils are strongly fragmented.
M0-8B	Crinoid-packstone with a micritic matrix. Fossils are represented by very numerous crinoid ossicles and fragmented brachiopods and molluscs. Less numerous are smooth-shelled ostracods, echinoids spines, and fragments of smooth-shelled ostracods. Additionally, single small brachiopods, fragments of bryozoans, calcispheres and some problematic structures, probably <i>Microcodium</i> . Many fossils are strongly fragmented.
M0-5	Bioclastic packstone with a micritic matrix, locally slightly neomorphosed. Fossils consist of crinoid ossicles and fragments of crinoids, fragmented Tabulata corals, brachiopods and molluscs. Other fossils are represented by smooth-shelled ostracods, gastropods, amphiporoids, and single calcispheres, sponge spicules and tentaculites. Fossils are strongly fragmented.
M0-4C	Crinoid packstone with a micritic matrix. Fossils are represented by very numerous crinoid ossicles and fragments of crinoids, numerous fragmented brachiopods, bryozoans, Tabulata and Rugosa corals, trilobites, and ostracods. Less numerous are smooth-shelled ostracods, calcispheres, and small brachiopods and sponge spicules. Fossils are strongly fragmented.
M0-2	Bioclastic packstone with a partly neomorphosed matrix, with very numerous fragmented crinoids, brachiopods and molluscs. Numerous fragments of tabulate corals, smooth-shelled ostracods, calcispheres and numerous gastropods. Single echinoid spines and fragments bryozoans occur. Fossils are strongly fragmented. Some of the bioclasts (especially crinoids) have microendolithic borings.
M0-1	Bioclastic packstone with a partly neomorphosed matrix, with peloids. Fossils are represented by numerous crinoid ossicles and fragmented crinoids, fragmented brachiopods and molluscs. Other fossils are represented by smooth-shelled ostracods, numerous calcispheres, e.g., <i>Parathuramina</i> , gastropods, foraminifers, echinoid spines, fragments of trilobites, bryozoans and tabulate corals. Fossils are strongly fragmented. Some of the bioclasts (especially crinoids) have microendolithic borings.

## Appendix 3

Habitats in the Pre-Taghanic (Givetian, Middle Devonian) muddy carbonate ramp at Miłoszów (Holy Cross Mountains, Poland): geochemical and microfacies evidence.

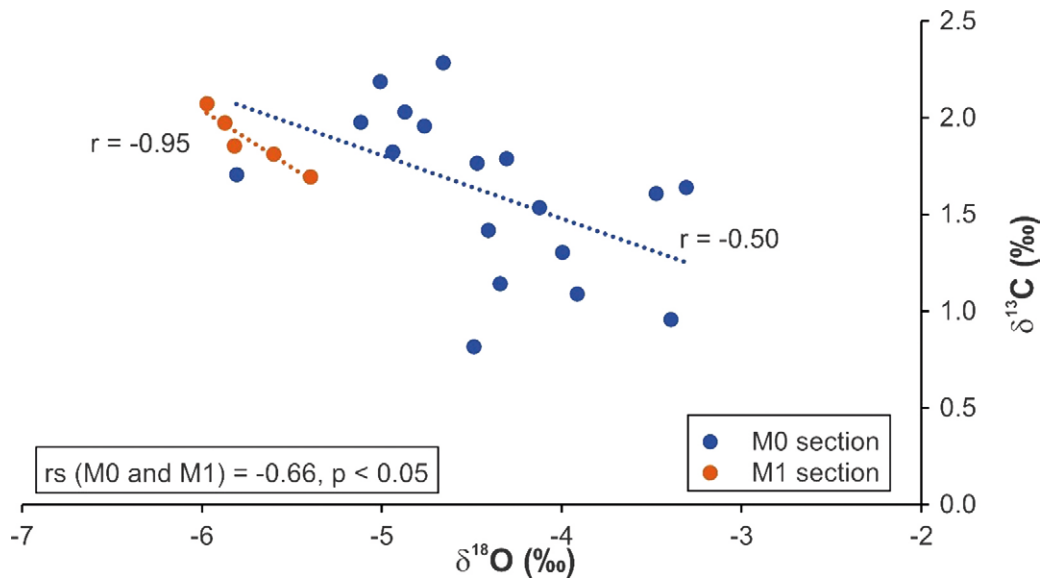


**Fig. A1.** Cross-plot of carbonate carbon and oxygen isotope data from the M1 and M0 sections. Spearman rank correlation ( $r_s$ ) and Pearson correlation ( $r$ ) coefficients,  $p$ -values below 0.05.

